JNKs protect from cholestatic liver disease progression by modulating Apelin signalling

Authors

Mohamed Ramadan Mohamed, Johannes Haybaeck, Hanghang Wu, Huan Su, Matthias Bartneck, Cheng Lin, Mark V. Boekschoten, Peter Boor, Benjamin Goeppert, Christian Rupp, Pavel Strnad, Roger J. Davis, Francisco Javier Cubero, Christian Trautwein

Correspondence

ctrautwein@ukaachen.de (C. Trautwein).

Graphical abstract

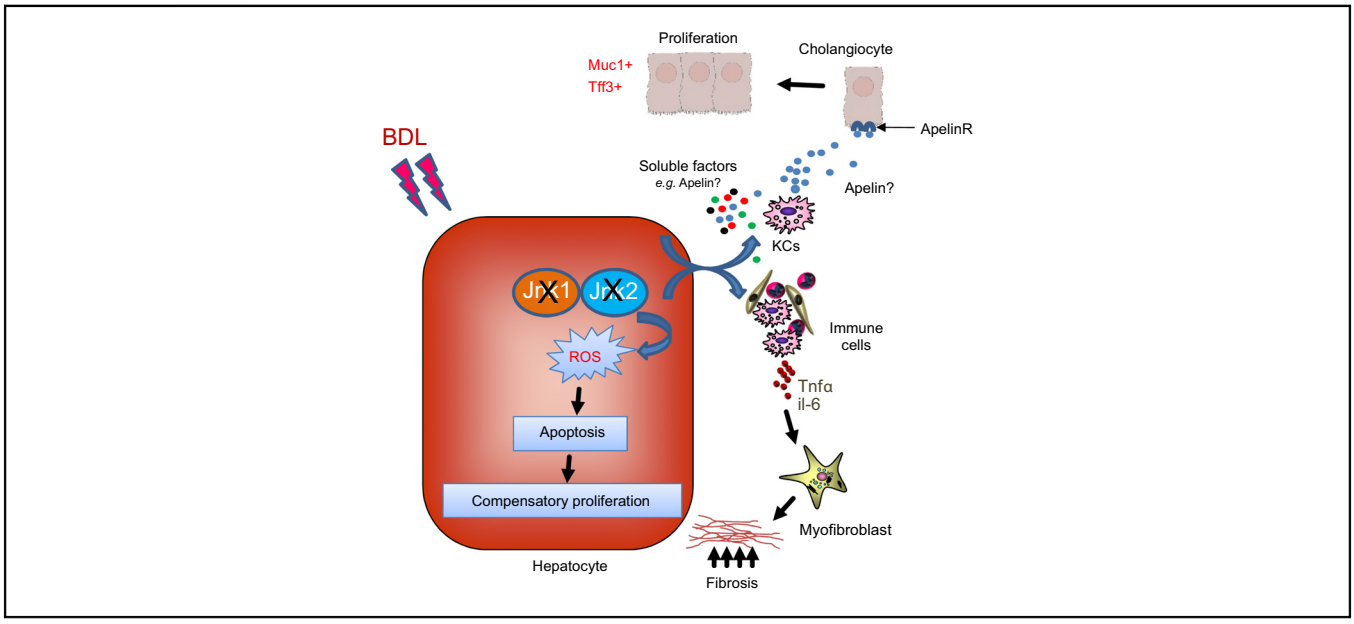

Highlights

- JNK is highly activated in hepatic cholestasis and positively correlates with cholestasis activity in humans.
- *Jnk1* and *Jnk2* cooperate in hepatocytes to prevent experimental cholestasis.
- *Jnk1/2* deletion triggered oxidative stress burst, loss of mucus homoeostasis, and upregulated the IL-6 and Apelin signalling pathways.
- Inhibiting Apelin signalling mitigates bile duct ligation-induced liver injury and fibrosis in *Jnk*-deficient mice.
- *siRNA* targeting *Jnk1/2* knockdown in wild-type mice recapitulates the $Jnk1^{\Delta hepa}/2^{\Delta hepa}$ phenotype after bile duct ligation.

Impact and Implications

The cell-specific function of *Jnk* genes during cholestasis has not been explicitly explored. In this study, we showed that combined *Jnk1/2*, but not *Jnk2* deficiency, in hepatocytes exacerbates liver damage and fibrosis by enhancing Apelin signalling, which contributes to cholestasis progression. Combined cell-specific Jnk targeting may be a new molecular strategy for treating cholestatic liver disease.

https://doi.org/10.1016/j.jhepr.2023.100854

Research article

JHEP|Reports

JNKs protect from cholestatic liver disease progression by modulating Apelin signalling

Mohamed Ramadan Mohamed,[1] Johannes Haybaeck,[2,3,4] Hanghang Wu,[5] Huan Su,[1] Matthias Bartneck,[1] Cheng Lin,[1] Mark V. Boekschoten,[6] Peter Boor,[7] Benjamin Goeppert,[8] Christian Rupp,[9] Pavel Strnad,[1] Roger J. Davis,[10] Francisco Javier Cubero,[5,11,12,†] Christian Trautwein[1,*,†]

[1]*Department of Internal Medicine III, University Hospital, RWTH Aachen, Aachen, Germany;* [2]*Institute of Pathology, Neuropathology and Molecular Pathology, Medical University of Innsbruck, Innsbruck, Austria;* [3]*Diagnostic and Research Center for Molecular BioMedicine, Institute of Pathology, Medical University of Graz, Graz, Austria;* [4]*Department of Pathology, Medical Faculty, Otto-von-Guericke University Magdeburg, Magdeburg, Germany;* [5]*Department of Immunology, Ophthalmology and ENT, Complutense University School of Medicine, Madrid, Spain;* [6]*Nutrition, Metabolism and Genomics Group, Division of Human Nutrition and Health, Wageningen University, Wageningen, The Netherlands;* [7]*Institute of Pathology and Department of Nephrology, University Hospital, RWTH Aachen, Aachen, Germany;* [8]*Institute of Pathology, University Hospital Heidelberg, Heidelberg, Germany;* [9]*Department of Internal Medicine IV, University Hospital Heidelberg, Heidelberg, Germany;* [10]*Howard Hughes Medical Institute and University of Massachusetts Medical School, Worcester, MA, USA;* [11]*Instituto de Investigación Sanitaria Gregorio Marañón (IiSGM), Madrid, Spain;* [12]*Centro de Investigación Biomédica en Red de Enfermedades Hepáticas y Digestivas (CIBEREHD), Madrid, Spain*

JHEP Reports **2023.** https://doi.org/10.1016/j.jhepr.2023.100854

Background & Aims: Cholestatic liver injury is associated with c-Jun N-terminal kinases (JNK) activation in distinct cell types. Its hepatocyte-specific function during cholestasis, however, has not yet been established. Therefore, in our present study, we investigated the role of JNK1/2 during cholestasis and dissected its hepatocyte-specific function.

Methods: A cohort of patients with primary biliary cholangitis (n = 29) and primary sclerosing cholangitis (n = 37) was examined. Wild-type, hepatocyte-specific knockout mice for *Jnk2* ($Jnk2^{\Delta hepa}$) or *Jnk1* and *Jnk2* ($Jnk1^{\Delta hepa}/2^{\Delta hepa}$) were generated. Mice were subjected to bile duct ligation (BDL) or carbon tetrachloride (CCl_4) treatment. Finally, Apelin signalling was blocked using a specific inhibitor. As an interventional approach, *Jnk1/2* were silenced in wild-type mice using lipid nanoparticles for small interfering RNA delivery.

Results: JNK activation was increased in liver specimens from patients with chronic cholestasis (primary biliary cholangitis and primary sclerosing cholangitis) and in livers of $Mdr2^{-/-}$ and BDL-treated animals. In $Jnk1^{\Delta hepa}/2^{\Delta hepa}$ animals, serum transaminases increased after BDL, and liver histology demonstrated enhanced cell death, compensatory proliferation, hepatic fibrogenesis, and inflammation. Furthermore, microarray analysis revealed that hepatocytic *Jnk1/2* ablation induces JNK-target genes involved in oxidative stress and Apelin signalling after BDL. Consequently, blocking Apelin signalling attenuated BDL-induced liver injury and fibrosis in $Jnk1^{\Delta hepa}/2^{\Delta hepa}$ mice. Finally, we established an interventional small interfering RNA approach of selective *Jnk1/2* targeting in hepatocytes *in vivo*, further demonstrating the essential protective role of *Jnk1/2* during cholestasis.

Conclusions: *Jnk1* and *Jnk2* work together to protect hepatocytes from cholestatic liver disease by controlling Apelin signalling. Dual modification of JNK signalling in hepatocytes is feasible, and enhancing its expression might be an attractive therapeutic approach for cholestatic liver disease.

Impact and Implications: The cell-specific function of *Jnk* genes during cholestasis has not been explicitly explored. In this study, we showed that combined *Jnk1/2*, but not *Jnk2* deficiency, in hepatocytes exacerbates liver damage and fibrosis by enhancing Apelin signalling, which contributes to cholestasis progression. Combined cell-specific Jnk targeting may be a new molecular strategy for treating cholestatic liver disease.

Introduction

Cholestatic liver injury is a major cause of liver fibrosis and, subsequently, cirrhosis in patients with chronic liver disease. In addition to mechanical obstruction of the common bile duct, for example, through bile stones or carcinomas, especially primary biliary cholangitis (PBC) and primary sclerosing cholangitis (PSC) frequently trigger biliary cirrhosis and finally might require liver transplantation.[1] Experimentally, surgical ligation of the common bile duct (BDL) has become the most prominent experimental model not only to induce obstructive cholestasis but also

Keywords: c-Jun N-terminal kinases (JNK); Cholestasis; Fibrosis; Hepatocytes; Apelin.
Received 22 September 2022; received in revised form 3 July 2023; accepted 7 July 2023; available online 18 July 2023

† These authors contributed equally.

* Corresponding author. Address: Department of Internal Medicine III, University Hospital, RWTH Aachen, Pauwelsstraße, 30, Aachen 52074, Germany. Tel./fax: +49 241 808 0866.
E-mail address: ctrautwein@ukaachen.de (C. Trautwein).

to thoroughly analyse the mechanisms triggering cholestasis. BDL induces liver fibrosis and is characterised by biliary epithelial cell (BEC) proliferation, activation of portal myofibroblasts, and massive deposition of extracellular matrix. Therefore, BDL mimics various aspects of the complex mechanisms leading to hepatic inflammation, fibrosis, and cirrhosis in patients with cholestasis.[2] Indeed, multiple signalling pathways have been reported to be implicated in the pathogenesis of hepatic cholestasis including c-Jun-N-terminal kinase (JNK) signalling.

JNK is a mitogen-activated protein kinase (MAPK) family member. There are three *Jnk* genes in mammals: *Jnk1, Jnk2*, and *Jnk3* (encoded by *MAPK8, MAPK9, and MAPK10*, respectively). *Jnk1* and *Jnk2* are expressed in almost all cells, including liver parenchymal cells, whereas *Jnk3* is mainly expressed in the brain, heart, and testis.[3,4] We and others investigated the potential role of *Jnk* for liver fibrogenesis.[5–7] In particular, Kluwe *et al.*[5] reported that $Jnk1^{-/-}$ mice were protected against hepatic fibrosis, whereas fibrogenesis was increased in *Jnk2*-deficient animals. Concomitantly, we showed that *Jnk1* activation mediates transactivation and inhibits apoptosis of hepatic stellate cells (HSCs) during murine liver fibrosis.[7]

However, before patients with cholestasis and fibrosis can be offered an effective treatment, selective inhibition of a specific gene (*e.g. Jnk*) or complete blockade of JNK in a specific cell or tissue needs to be thoroughly investigated. In hepatocytes, *Jnk1* and *Jnk2* appear to have combined effects in protecting mice from chronic liver disease of different aetiologies, whereas the deleterious functions of *Jnk* genes might be restricted to the non-parenchymal cell (NPC) compartment.[8–11]

In the present study, we aimed to characterise the relevance of *Jnk* activation in PBC and PSC. We generated hepatocyte-specific *Jnk1/2* double knockout mice for functional studies to analyse the tissue-specific role of *Jnk* in hepatocytes. We performed a comprehensive analysis and here describe cell-specific strategies to target *Jnk* in cholestatic liver disease using our experimental approach. As a result, targeting JNK may be an effective treatment for cholestatic liver disease, whereas pan-JNK inhibition may have negative side effects.

Materials and methods

Human samples

Human formalin-fixed and paraffin-embedded liver specimens were obtained from patients with PSC and PBC (n = 37 and n = 29, respectively) who underwent liver biopsy, resection, or transplantation. Control liver tissues without histological signs of inflammation or fibrosis (n = 5) were obtained from individuals undergoing liver resection as a result of metastasis. The samples were collected retrospectively at the Institute of Pathology, RWTH Aachen University, Aachen, Germany; the Department of Pathology, Otto-von-Guericke University Magdeburg, Germany; the Institute of Pathology, Neuropathology and Molecular Pathology of the University of Innsbruck, Austria; and the tissue bank of the Pathology Institute of the University of Heidelberg under the approval of the local ethics committees (No. 61/18 Magdeburg; No 1115/2019 Innsbruck; No. EK166-12 Aachen; and No. S-043/2011 Heidelberg). Three board-certified liver pathologists blinded to the clinical details confirmed the diagnosis histologically (JH, PB, and BG).

Generation of mice and animal experiments

Alb-Cre mice with a C57BL/6 background were purchased from The Jackson Laboratory (Bar Harbor, ME, USA). Hepatocyte-specific *Jnk2* ($Jnk2^{\Delta hepa}$) and *Jnk1/2* ($Jnk1^{\Delta hepa}/Jnk2^{\Delta hepa}$) mice were generated by crossing $Jnk2^{LoxP/LoxP}$ and $Jnk1^{LoxP/LoxP}/Jnk2^{LoxP/LoxP}$, respectively, with *Alb-Cre*-transgenic mice. Animal experiments were carried out according to the German and Spanish legal requirements and animal protection law, and approved by the authority (LANUV, Germany, No./AZ: 84-02.04.2016.A080; and Spain, PROEX 125-1/20). Induction of liver fibrosis was performed in 8- to 10-week-old age-matched male mice (six to seven animals were included per time point and mouse strain) by ligating the common bile duct (BDL) for 2 and 28 days. Control animals (four per group) were opened and immediately closed (sham). To support the findings from $Jnk1^{\Delta hepa}/Jnk2^{\Delta hepa}$ mice, we treated C57BL/6 wild-type (WT) mice with lipid nanoparticles (LNPs) carrying *small interfering RNAs* (siRNAs) against *Jnk1* and *Jnk2* to knock down *Jnk1/2* in hepatocytes followed by BDL for 2 days. For functional study, $Jnk1^{f/f}/2^{f/f}$ and $Jnk1^{\Delta hepa}/2^{\Delta hepa}$ mice were treated with the Apelin receptor (ApelinR) antagonist (ML221) during BDL for 1 week (see the Supplementary information).

For details on methodology, please see the Supplementary information.

Results

Activation of JNK in human cholestatic liver disease

Previously, we showed that JNK is activated in inflammatory cells and myofibroblasts in patients with metabolic liver disease.[7] However, cholestatic liver disorders, including PBC and PSC, differ in their pathogenesis.[12] Hence, we here investigated the relevance of JNK in human and experimental cholestatic liver disease.

Patients with PBC (n = 29) and PSC (n = 37) (Table 1) were included. Representative H&E staining shows the typical histological liver appearance of PBC with progressive destruction of small and medium-sized intrahepatic bile ducts, bile duct loss, lymphoid cell infiltration, fibrosis ranging from limited portal tracts to liver cirrhosis and PSC, a chronic cholestatic disorder with progressive fibro-obliterative destruction of segments of the biliary tree. The diseased were compared with healthy control livers (Fig. 1A). Here, we found strong phosphorylated JNK (pJNK) immunoreactivity in livers of patients with PBC and PSC compared with healthy controls. Interestingly, strong JNK activation was located in inflamed bile duct areas including hepatocytes, the biliary epithelium, and other cells within the portal fields, whereas pJNK staining was reduced or absent within noninflamed bile ducts areas (Fig. 1B and Fig. S1A), suggesting an association between JNK activation and cholestatic liver disease development.

Quantification of pJNK-positive areas revealed a significant increase of JNK activation in patients with PBC and PSC compared with controls (Fig. 1C). As shown in Fig. 1D and Fig. S1B, Western blot analysis showed higher JNK expression in diseased livers compared with healthy livers. In addition, pJNK expression as a marker of JNK activation was significantly increased in livers of patients with PBC and PSC compared with healthy tissue (Fig. 1E and Fig. S1C).

Alkaline phosphatase (AP) is a reliable and diagnostic marker of disease activity in patients with PBC and PSC.[13] Here, we found a correlation between pJNK-positive areas and increased AP serum levels (Fig. 1F).

Earlier results linked JNK1/2 activation and liver fibrosis.[5,7,8] This led us to investigate whether there is a correlation

Table 1. Clinicopathological characteristics of patients with PSC and PBC.

Variables	Patients with PSC (n = 37)	Patients with PBC (n = 29)
Age (years), mean ± SD	40.16 ± 13.2	56.14 ± 9.41
Sex, n (%)		
Female	9 (24.3)	26 (89.66)
Male	28 (75.7)	3 (10.34)
AP (40–130 U/L), mean ± SD	261.38 ± 187.61	306.83 ± 204.58
GGT (<60 U/L), mean ± SD	290.73 ± 282.58	355.69 ± 511.65
AST (<50 U/L), mean ± SD	124.14 ± 185.75	83.62 ± 132.51
ALT (<50 U/L), mean ± SD	155.08 ± 167.92	84.69 ± 91.22
Total bilirubin (<1.2 mg/dl), mean ± SD	2.09 ± 2.42	1.90 ± 3.72
Cholangitis activity, n (%)		
CA0	3 (8.1)	
CA1	16 (43.2)	9 (31)
CA2	10 (27)	6 (20.7)
CA3	8 (21.6)	14 (48.3)
Hepatitis activity, n (%)		
HA0	3 (8.1)	1 (.4)
HA1	18 (48.6)	8 (27.6)
HA2	12 (32.4)	13 (44.8)
HA	4 (10.8)	7 (24.1)
Score A (fibrosis), n (%)		
Stage 0	3 (8.1)	
Stage 1	10 (27)	11 (37.9)
Stage 2	9 (24.3)	8 (27.6)
Stage 3	15 (40.5)	10 (4.5)
Score B (bile duct loss), n (%)		
Stage 0	5 (13.5)	
Stage 1	9 (24.3)	9 (31)
Stage 2	15 (40.5)	14 (48.3)
Stage 3	8 (21.6)	6 (20.7)
Score C (deposition of orcein-positive granules), n (%)		
Stage 0	24 (64.9)	15 (51.7)
Stage 1	9 (24.3)	9 (31)
Stage 2	1 (2.7)	2 (6.9)
Stage 3	3 (8.1)	3 (10.3)
Staging of PBC and PSC based on Nakanuma *et al.*[36], n (%)		
Stage 1	3 (8.1)	
Stage 2	9 (24.3)	5 (17.2)
Stage 3	10 (27)	10 (34.5)
Stage 4	4 (10.8)	4 (13.8)
Stage 5	2 (5.4)	4 (13.8)
Stage 6	6 (16.2)	5 (15.2)
Stage 7	1 (2.7)	
Stage 8	1 (2.7)	1 (3.4)
Stage 9	1 (2.7)	
Ludwig's staging (fibrosis, cholangitis, and hepatitis)[37], n (%)		
Stage 1	5 (13.5)	2 (6.9)
Stage 2	7 (18.9)	11 (37.9)
Stage 3	6 (16.2)	8 (27.6)
Stage 4	19 (51.4)	8 (27.6)

Data are presented as mean ± SD or n (%).
ALT, alanine aminotransferase; AP, alkaline phosphatase; AST, aspartate aminotransferase; GGT, gamma-glutamyltransferase; PBC, primary biliary cholangitis; PSC, primary sclerosing cholangitis.

between pJNK expression in PBC and PSC livers and fibrosis staging (F0–F3). As expected, pJNK expression was significantly increased in different stages of fibrotic PBC and PSC livers compared with healthy control livers. However, there was no stage-dependent increase (Fig. 1G). The detailed analysis demonstrated increased JNK activation in both cholangiocytes and NPCs and significantly correlated with the degree of liver fibrosis in patients with cholestasis (Fig. 1H and Fig. S2D and E). Although the number of hepatocyte-positive cells was increased in fibrotic livers (F1–F3) compared with F0, the number of hepatocyte-positive cells was inversely correlated with the degree of liver fibrosis (Fig. S2D and F).

Next, we compared the spatial distribution of pJNK and *alpha-smooth muscle actin* (αSMA) expression in livers of patients with PSC and PBC. Interestingly, double αSMA and pJNK-positive HSCs were observed (Fig. 1I). However, apart from HSC-positive cells, co-staining of pJNK–cytokeratin 19 (CK19) demonstrated cholangiocytes and hepatocytes, among the pJNK-positive cells, with the highest density in the periportal area (Fig. 1J).

Enhanced *Jnk* expression and activation in murine cholestasis

The finding that JNK is activated in different cell types, for example, hepatocytes and NPCs in livers of patients with cholestasis suggested that JNK might have different functions during disease progression. Thus, we aimed to define the cell-type-specific function of JNK in cholestatic liver disease.

Indeed, as found in human cholestatic livers, we found enhanced *Jnk1* and *Jnk2* mRNA expression in livers of BDL-treated WT ($Jnk1^{f/f}/2^{f/f}$) mice compared with sham-operated WT controls (Fig. S2C), suggesting a functional role of *Jnk1* and *Jnk2* during cholestasis.

Next, we studied JNK activation in two murine models of cholestasis – $Mdr2^{-/-}$ animals and WT mice following BDL. As shown in Fig. 2A and B, JNK protein expression was comparable in diseased and healthy livers**.** However, in BDL-treated and *Mdr2*-deficient mice, we found increased pJNK expression, strengthening the link between JNK activation and cholestasis. pJNK immunostaining of liver sections using both models uniformly revealed increased intensity of pJNK staining in the periportal areas, which decreased or is almost absent in the central vein area. Notably, pJNK staining was visible in the biliary epithelium, hepatocytes, and NPCs in the vicinity of bile ducts of cholestatic livers compared with respective controls (Fig. 2C). Moreover, JNK activation was demonstrated in Kupffer cells (KCs) as seen by co-staining with CLEC4F (Fig. 2D). As a result, our findings clearly showed that mouse cholestasis reflects the human JNK activation phenotype. We primarily focused on the BDL model to define the functional role of JNK during cholestasis.

Hepatocyte-specific *Jnk2* deletion does not change the course of BDL-induced liver injury

Our previous work demonstrated that *Jnk1* in hepatocytes has no impact on acute and chronic hepatic injury during experimental liver fibrosis.[7] We evaluated the relevance of *Jnk2* in hepatocytes ($Jnk2^{\Delta hepa}$) for BDL during cholestasis. Deletion of *Jnk2* in hepatocytes was confirmed by genotyping PCR, *reverse transcription PCR*, and Western blot analyses (Fig. S2A–C). Twenty-eight days after BDL, $Jnk2^{\Delta hepa}$ livers showed no obvious macroscopic or microscopic differences compared with controls ($Jnk2^{f/f}$) (Fig. S2D and E).

Moreover, hepatic fibrosis assessed by Sirius Red (SR) staining and mRNA expression of *collagen 1A1 (Col1A1)* and *αsma* as well as serum levels of alanine aminotransferase (ALT) and bilirubin were comparable between both groups (Fig. S2F–H).

Overall, our findings suggest compensatory crosstalk between *Jnk1* and *Jnk2* in hepatocytes as hepatocyte-specific *Jnk2* deletion did not significantly influence liver damage and fibrosis following BDL.

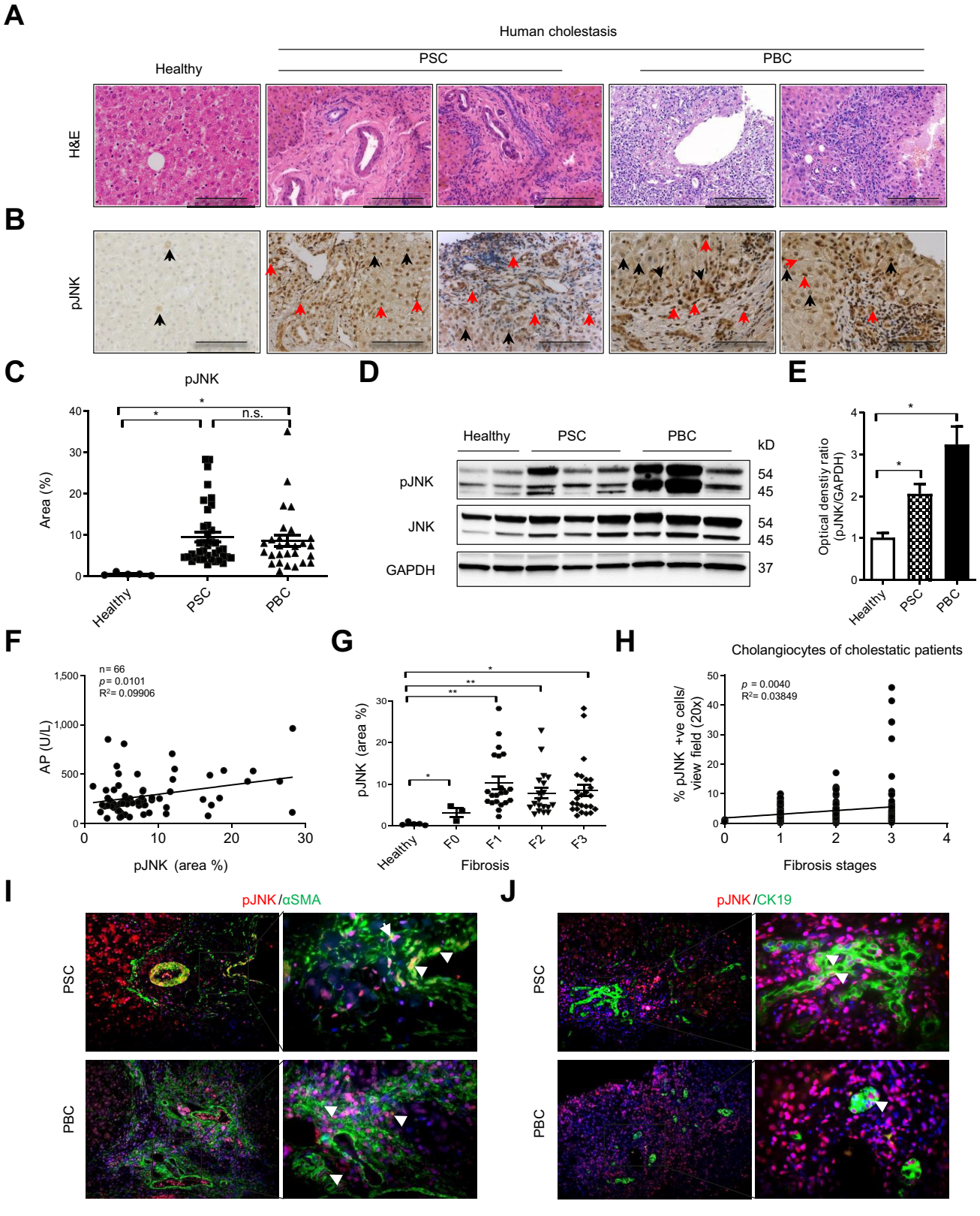

Fig. 1. JNK activation in human cholestasis. (A) Liver paraffin sections from healthy patients (n = 5) and patients with cholestasis with PSC (n = 37) and PBC (n = 29) stained with H&E show the typical histological pattern of human PSC and PBC. (B) Representative immunohistochemistry staining for pJNK of the same human liver sections. Scale bar = 100 μm. Black arrows indicate pJNK-positive hepatocytes, whereas red arrows indicate positive NPCs. (C) The percentage of pJNK-positive stained areas was measured using ImageJ® software (National Institutes of Health, Bethesda, MD, USA). (D) Liver extracts from individuals with PSC

Generation of hepatocyte-specific *Jnk1/Jnk2* double knockout mice

Mice with constitutive combined *Jnk1* and *Jnk2* deletion die during embryonal development.[14] To test the hypothesis that *Jnk1* and *Jnk2* compensate for each other, we generated hepatocyte-specific *Jnk1/Jnk2* knockout mice ($Jnk1^{\Delta hepa}/2^{\Delta hepa}$) using *Alb-Cre* transgenic mice as confirmed on the DNA and RNA level as well as on the protein level by Western blot analysis (Fig. S2A–C). Hepatic parameters did not significantly differ between $Jnk1^{\Delta hepa}/2^{\Delta hepa}$ mice and their WT control ($Jnk1^{f/f}/2^{f/f}$) littermates under basal conditions or in animals that underwent sham surgery, indicating that there was no hepatic phenotype up to 4 months of age (data not shown), supporting previously published findings.[11]

Loss of *Jnk1* and *Jnk2* in hepatocytes aggravates BDL-induced acute and chronic liver damage

Next, we examined the relevance of hepatocytic *Jnk1/2* deficiency for acute liver injury after BDL treatment. When compared with their WT littermates ($Jnk1^{f/f}/2^{f/f}$), $Jnk1^{\Delta hepa}/2^{\Delta hepa}$ mice displayed significantly higher blood ALT and *aspartate aminotransferase* (AST) levels 48 h after BDL (Fig. 2E). Moreover, BDL triggered necrotic areas in the hepatic parenchyma of $Jnk1^{f/f}/2^{f/f}$ livers, which was significantly exacerbated in $Jnk1^{\Delta hepa}/2^{\Delta hepa}$ livers, coinciding with the observed bile infarcts on the liver surface (Fig. 2F). SR staining, and *αsma* and *Col1A1* mRNA levels were used to study liver fibrosis, and they revealed a tendency towards higher expression in $Jnk1^{\Delta hepa}/2^{\Delta hepa}$ livers than in $Jnk1^{f/f}/2^{f/f}$ livers (data not shown).

Selective expression of *Alb-Cre* transgene in hepatocytes but not in cholangiocytes of $Jnk1^{\Delta hepa}/2^{\Delta hepa}$ livers was tested in serial liver sections from BDL-treated mice by immunostaining for pJNK or CK19 (Fig. S3A and B). Of note, BDL in $Jnk1^{f/f}/2^{f/f}$ livers was associated with JNK activation as indicated by positive pJNK staining in different hepatic cell types including hepatocytes, cholangiocytes, and NPCs surrounding CK19-positive cholangiocytes (Fig. S3A). By contrast, almost no pJNK-positive hepatocytes were detected in $Jnk1^{\Delta hepa}/2^{\Delta hepa}$ livers but in other cells (Fig. S3B). Strikingly, CK19 immunostaining of serial liver sections of $Jnk1^{\Delta hepa}/2^{\Delta hepa}$ livers revealed that CK19-postive cells overlapped mostly with pJNK-positive cells (Fig. S3B), showing JNK activation in cholangiocytes of $Jnk1^{\Delta hepa}/2^{\Delta hepa}$ livers. These results suggest that the *Alb-Cre* promotor mediates efficient excision of floxed genes in hepatocytes but not in cholangiocytes, supporting previously reported findings.[15]

In vitro, compared with $Jnk1^{f/f}/2^{f/f}$ hepatocytes, isolated hepatocytes from $Jnk1^{\Delta hepa}/2^{\Delta hepa}$ mice showed more susceptibility to cell death, as indicated by less viability after isolation and increased transaminases in the culture medium after 3 and 16 h (Fig. S4A–C). However, treatment of hepatocytes with cholic acid (CA) or deoxycholic acid (DCA) for 48 h exacerbated cell death in both groups, which was more prominent in $Jnk1^{\Delta hepa}/2^{\Delta hepa}$ hepatocytes, as indicated by increased dead cells and elevated medium ALT and AST levels (Fig. S4D–F). Next, we studied the functional impact of hepatocytic *Jnk1/Jnk2* deletion for chronic cholestasis (28 days after BDL). No significant difference in weight loss after BDL was found between $Jnk1^{\Delta hepa}/2^{\Delta hepa}$ and $Jnk1^{f/f}/2^{f/f}$ animals (data not shown). However, 28 days after BDL, serum AST and ALT levels were significantly increased in $Jnk1^{\Delta hepa}/2^{\Delta hepa}$ mice compared with $Jnk1^{f/f}/2^{f/f}$ mice, whereas sham-treated groups showed no change from baseline (Fig. 3A). No significant difference in bilirubin serum levels were evident between BDL-treated groups (Fig. 3A).

Macroscopic examination of $Jnk1^{\Delta hepa}/2^{\Delta hepa}$ BDL-treated livers showed prominent yellowish nodules on their surface, whereas only small dots were found in controls (Fig. 3B). Concomitantly, H&E staining showed bile infarcts that vary in size ranging from areas with few hepatocytes to large areas, sometimes with a broad subcapsular affection, reflecting the macroscopic findings. In $Jnk1^{\Delta hepa}/2^{\Delta hepa}$ livers, bile infarcts were typically four times larger. This was connected to a large rise in CK19-positive cells near the original bile ducts in comparison with controls, indicating oval cell activation (Fig. 3C and D).

Massive cell death and compensatory proliferation are characteristics of JNK-deficient livers after BDL

The accumulation of toxic bile salts within the liver occurring after BDL causes hepatocellular injury via apoptosis and necrosis. Thus, increased liver injury in $Jnk1^{\Delta hepa}/2^{\Delta hepa}$ animals after BDL raised the question for the mode of cell death. Immunostaining for cleaved caspase 3 (Cl. Casp-3) revealed a significant increase of positive cells in $Jnk1^{\Delta hepa}/2^{\Delta hepa}$ livers compared with controls after BDL (Fig. 3E and F). Cl. Casp-3-positive cells were especially grouped around bile ducts and were not found in respective sham-treated animals (Fig. 3E and Fig. S5A). Increased apoptosis in $Jnk1^{\Delta hepa}/2^{\Delta hepa}$ livers was associated with a higher rate of cell proliferation in the vicinity of bile ducts and necrotic areas as shown by Ki-67 staining compared with that in controls (Fig. 3E and F and Fig. S5A).

Hepatocytic loss of JNK promotes immune cell infiltration to the liver

We next analysed the impact of BDL-induced liver injury on immune cell infiltration. CD45 staining showed a marked increased recruitment of hepatic leukocytes in $Jnk1^{f/f}/2^{f/f}$ livers, which was significantly enhanced in $Jnk1^{\Delta hepa}/2^{\Delta hepa}$ livers, predominantly in the periductal area (Fig. 4A and B and Fig. S5B). Further analysis of liver sections showed that F4/80- and CD11b-positive macrophages are the prominent cell types, and these immune cells are significantly increased in $Jnk1^{\Delta hepa}/2^{\Delta hepa}$ livers compared with control livers after BDL (Fig. 4A and B and Fig. S5B). The increase in immune cell infiltration was consistent with the increased expression of the inflammatory cytokine *tumour necrosis factor α* (*Tnfα*) and *interleukin* (*il*)-6 mRNA found

(n = 3) or PBC (n = 3) in addition to healthy control patients (n = 2) were examined by immunoblot analysis using antibodies against GAPDH, JNK, and pJNK. (E) The density of the pJNK bands was quantified and compared with GAPDH intensity accordingly. The optical density of pJNK/GAPDH ratio in healthy controls was set to 1. (F) Linear regression analysis of pJNK-positive area *vs.* AP demonstrating that increased pJNK staining correlates with increased AP serum values. (G) Correlation between pJNK-positive area and stages of fibrotic PSC and PBC livers. Statistical evaluation was carried out by multicomparison one-way ANOVA followed by *post hoc* Bonferroni's test among three or more groups. Comparisons of two groups were analysed using an unpaired, two-tailed Student *t* test. Values are represented as mean ± SEM (*n*, not significant; $^{*}p$ <0.05; $^{**}p$ <0.01). (H) Correlation between pJNK-positive cholangiocytes and the different fibrosis stages of PSC and PBC livers. Liver sections from patients with cholestasis were triple stained for pJNK (red), nuclei with DAPI (blue), and (I) αSMA (green) or (J) CK19 (green) followed by immunofluorescence microscopy. Arrows indicate double positive cells. αSMA, alpha-smooth muscle actin; AP, alkaline phosphatase; CK19, cytokeratin 19; JNK, c-Jun-N-terminal kinase; NPC, non-parenchymal cell; PBC, primary biliary cholangitis; PSC, primary sclerosing cholangitis; pJNK, phosphorylated JNK.

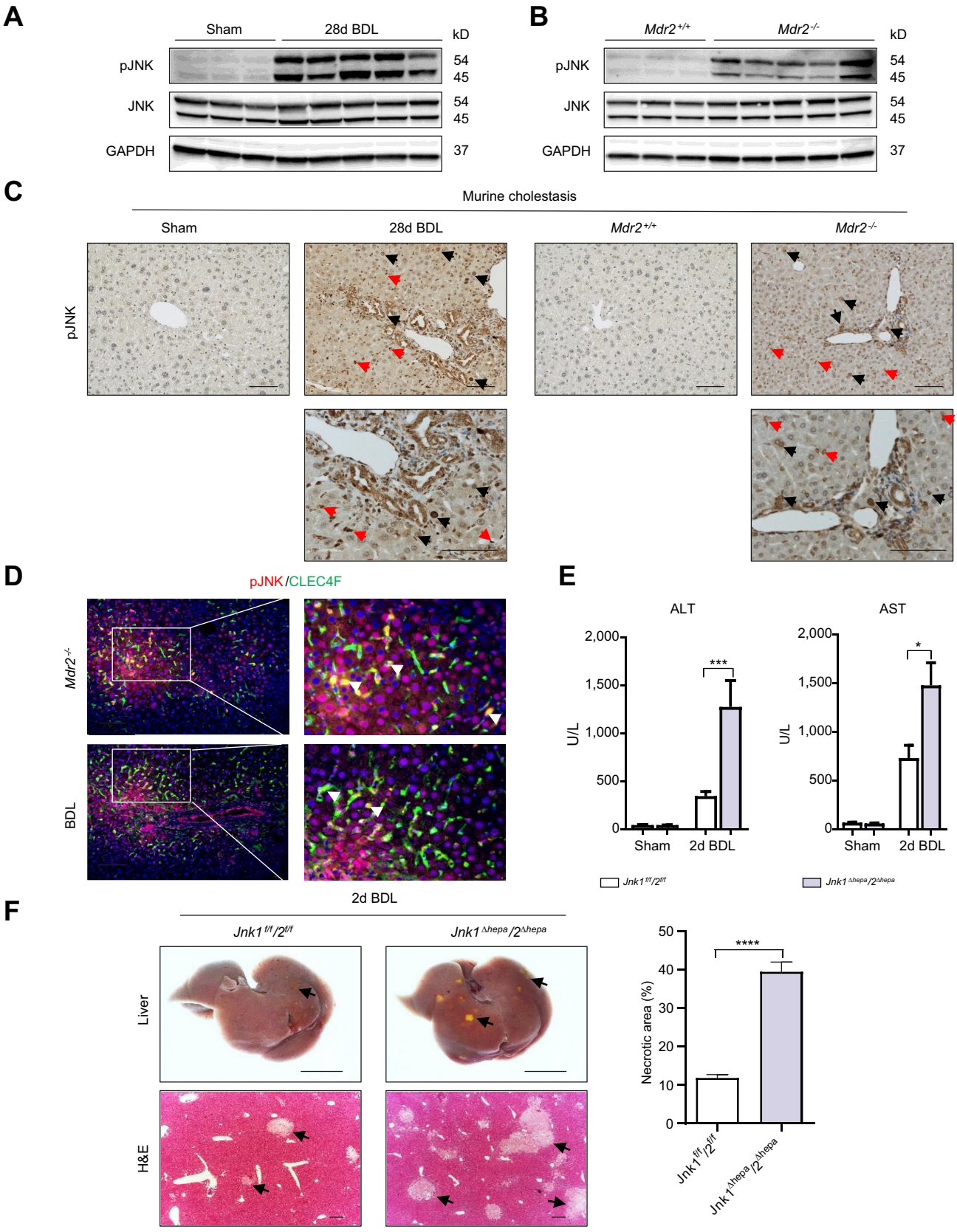

Fig. 2. Murine cholestasis triggers JNK activation and ablation of JNK1/2 in hepatocytes promotes acute cholestasis. (A, B) Liver extracts prepared from BDL-treated or *Mdr2*$^{-/-}$ mice (n = 5) and sham or WT mice (n = 3) were examined by immunoblot analysis using antibodies against GAPDH, JNK, and pJNK. (C) Representative immunohistochemistry staining for pJNK of liver sections from *Mdr2*$^{-/-}$ animal and BDL-treated non-transgenic mice are shown at different magnifications (20× in the upper panel and 40× in the lower panel; scale bar = 100 μm). *Mdr2*$^{+/+}$ and sham-operated mice were used as controls. Black arrows

in the liver of *Jnk1*$^{\Delta hepa}$/*2*$^{\Delta hepa}$ mice compared with *Jnk1*$^{f/f}$/*2*$^{f/f}$ mice (Fig. S5C).

Lack of JNK1/2 expression in hepatocytes triggers increased fibrogenesis

In *Jnk1*$^{\Delta hepa}$/*2*$^{\Delta hepa}$ animals, chronic cholestasis following BDL resulted in significant liver damage and inflammation. Thus, we investigated whether this affected fibrogenesis. *Jnk1*$^{f/f}$/*2*$^{f/f}$ SR-positive areas were used to measure periductal and partially bridging fibrosis in BDL-treated animals compared with sham-operated animals. *Jnk1*$^{\Delta hepa}$/*2*$^{\Delta hepa}$ livers displayed the most pronounced increase in SR-positive areas compared with controls following BDL (Fig. 4C and D and Fig. S5D).

This striking result was further confirmed by immunofluorescence for Col1A1, desmin, and αSMA (Fig. 4C–F and Fig. S5D and E). Col1A1, desmin, and αSMA protein expression analysis showed a significant increase in their expressions in *Jnk1*$^{\Delta hepa}$/*2*$^{\Delta hepa}$ livers compared with *Jnk1*$^{f/f}$/*2*$^{f/f}$ livers. mRNA transcripts for fibrosis-related genes, *Col1A1, αsma, matrix metalloproteinase* (*mmp*)*7*, and *mmp12*, were significantly higher in *Jnk1*$^{\Delta hepa}$/*2*$^{\Delta hepa}$ livers than in WT controls after BDL (Fig. S6A and B).

In summary, *Jnk1* and *Jnk2* compensate for each other during experimental cholestasis, although a combined loss in hepatocytes is detrimental.

Jnk1/2-dependent gene regulation during cholestatic liver injury

To investigate *Jnk1/2*-dependent pathways, we used Affymetrix GeneChip microarray analysis of *Jnk1*$^{f/f}$/*2*$^{f/f}$ (WT) and *Jnk1*$^{\Delta hepa}$/*2*$^{\Delta hepa}$ livers 28 days after BDL. Apelin and IL-17A were found to be the two most significantly altered pathways in response to *Jnk1/2* deletion in hepatocytes during cholestatic liver injury as assessed by Ingenuity Pathway Analysis (−5.0 >fold change >5.0). Next, we performed hierarchical clustering on genes that are significantly upregulated or downregulated in *Jnk1*$^{\Delta hepa}$/*2*$^{\Delta hepa}$ livers (Fig. 5A and B). Here, we found that hepatocytic *Jnk1* and *Jnk2* ablation dramatically downregulated expression of *Cxcl13* and *Fmo3* and increased levels of *Tff3, Fabp1, Mup1, Ces3,* and *Sucnr1* (Fig. 5B).

The validation of mRNA expression in *Jnk1*$^{\Delta hepa}$/*2*$^{\Delta hepa}$ and control livers confirmed significantly upregulated expression of *Cxcl13* and *Fmo3* and decreased expression of *Tff3, Fabp1*, and *Mup1* (Fig. S6C). Mucin 1 (Muc1) was considerably elevated in *Jnk1*$^{\Delta hepa}$/*2*$^{\Delta hepa}$ livers concurrently with Tff3 overexpression (Fig. 5C). To maintain and restore gastrointestinal mucosal homoeostasis, it is noteworthy that TFF3 is co-expressed with mucins.[15,16] In addition, *Jnk1*$^{\Delta hepa}$/*2*$^{\Delta hepa}$ livers exhibited an aggravation of reactive oxygen species, particularly 4-hydroxynonenal (Fig. 5D).

Analysis of microarray data revealed an increased expression of acute-phase response genes. Therefore, we investigated *Saa1, Saa2*, and *Saa3* mRNA levels in *Jnk1*$^{f/f}$/*2*$^{f/f}$ and *Jnk1*$^{\Delta hepa}$/*2*$^{\Delta hepa}$ mice. In JNK-deficient livers, there was a substantial upregulation of genes associated with the acute-phase response (Fig. 5E).

Ablation of JNK signalling in hepatocytes activates the Apelin–ApelinR axis

Consistent with the microarray results, the Apelin–ApelinR axis has been shown to play a crucial role in cholangiocyte proliferation and fibrogenesis.[16] mRNA expression levels of *Apelin* and its receptor were strongly increased in *Jnk1*$^{\Delta hepa}$/*2*$^{\Delta hepa}$ BDL-treated livers (Fig. 5F). Immunostaining for Apelin confirmed this finding. Apelin expression was upregulated in mice livers after BDL compared with sham-operated mice. However, *Jnk1*$^{\Delta hepa}$/*2*$^{\Delta hepa}$ livers exhibited significantly increased expression of Apelin. Notably, Apelin-positive cells were mainly cholangiocytes and NPCs within the portal field but less in hepatocytes (Fig. 6A).

Therefore, we next investigated the expression of *Apelin* and *ApelinR* in different liver cells. We isolated mRNA from hepatocytes, HSCs, and KCs of WT mice. Interestingly, significant *Apelin* and *ApelinR* expression was found in KCs (Fig. 6B). Hence, these results suggested that via a JNK-dependent pathway in NPCs, *Apelin* and *ApelinR* expression is increased when *Jnk1* and *Jnk2* are deleted in hepatocytes.

To test this hypothesis, *Jnk1*$^{f/f}$/*2*$^{f/f}$ and *Jnk1*$^{\Delta hepa}$/*2*$^{\Delta hepa}$ hepatocytes were isolated and cultured in the absence or presence of CA or DCA (Fig. 6C). Compared with *Jnk1*$^{f/f}$/*2*$^{f/f}$ hepatocytes, *Jnk1*$^{\Delta hepa}$/*2*$^{\Delta hepa}$ non-treated hepatocytes showed enhanced *Apelin* expression, which was further enhanced in bile acid (BA)-treated cells (Fig. 6D), suggesting a crucial role of hepatocytic JNK in regulating *Apelin* expression. By contrast, *ApelinR* expression was significantly reduced in response to Jnk deficiency in non-treated hepatocytes compared with *Jnk1*$^{f/f}$/*2*$^{f/f}$ hepatocytes, which further decreased upon BA treatment in both phenotypes. Given that *Jnk1*$^{\Delta hepa}$/*2*$^{\Delta hepa}$ hepatocytes showed high expression of *Apelin* (Fig. 6D), we tested whether hepatocytic JNK contributes to the upregulation of *Apelin* expression in KCs via a paracrine manner. Primary hepatocytes were isolated from *Jnk1*$^{\Delta hepa}$/*2*$^{\Delta hepa}$ and *Jnk1*$^{f/f}$/*2*$^{f/f}$ livers and cultured with or without CA and DCA for 48 h, and then the supernatant was transferred into the primary culture of KCs (Fig. 6C). Strikingly, we found that the supernatant from *Jnk1*$^{\Delta hepa}$/*2*$^{\Delta hepa}$ hepatocytes stimulated by CA or DCA promoted the expression of *Apelin and ApelinR* in KCs compared with that from BA-treated WT and non-treated controls (Fig. 6E). These results strongly suggested that probably Apelin and/or other secretory factors from BA-stimulated Jnk-deficient hepatocytes promote *Apelin* expression in KCs.

Next, we investigated whether increased *Apelin* expression in response to hepatocyte Jnk deficiency is specific to cholestatic models or is also prominent in toxic injury models such as carbon tetrachloride (CCl_4). We found that compared with *Jnk1*$^{f/f}$/*2*$^{f/f}$ CCl_4-treated mice, *Jnk1*$^{\Delta hepa}$/*2*$^{\Delta hepa}$ CCl_4-treated mice exhibited a significant increase in *Apelin* and *ApelinR* mRNA expression and Apelin staining (Fig. 6F and G). However, *Apelin* and *ApelinR* expression were more prominent in *Jnk1*$^{\Delta hepa}$/*2*$^{\Delta hepa}$ BDL-treated than in *Jnk1*$^{\Delta hepa}$/*2*$^{\Delta hepa}$ CCl_4-treated mice (Fig. S6D).

Apelin's relevance in human cholestasis has been recently proposed.[17] As a result, we stained liver sections of patients with PSC and PBC for Apelin. Apelin was significantly highly expressed

indicate pJNK-positive hepatocytes, whereas red arrows indicate positive NPCs. (D) Liver sections from *Mdr2*$^{-/-}$ and BDL-treated mice were triple stained for pJNK (red), nuclei with DAPI (blue), and CLEC4F (green) followed by immunofluorescence microscopy. Arrows indicate double positive cells. (E) *Jnk1*$^{f/f}$/*2*$^{f/f}$ and *Jnk1*$^{\Delta hepa}$/*2*$^{\Delta hepa}$ mice were subjected to 2 days of BDL (n = 6) or sham (n = 3). Serum AST and ALT levels were determined. (F) Macroscopic (upper panel) and microscopic (lower panel) appearance (scale bar = 1 cm) and sections of the liver from the same mice were stained with H&E (lower panel). The scale bar represents 100 μm. Necrotic areas were quantified. Statistical evaluation was carried out by multicomparison one-way ANOVA followed by *post hoc* Bonferroni's test among three or more groups. Comparisons of two groups were analysed using an unpaired, two-tailed Student *t* test. Values are represented as mean ± SEM (*p <0.05; ***p <0.001). ALT, alanine aminotransferase; AST, aspartate aminotransferase; BDL, bile duct ligation; JNK, c-Jun-N-terminal kinase; Mdr2, multidrug resistance 2; NPC, non-parenchymal cell; pJNK, phosphorylated JNK; WT, wild-type.

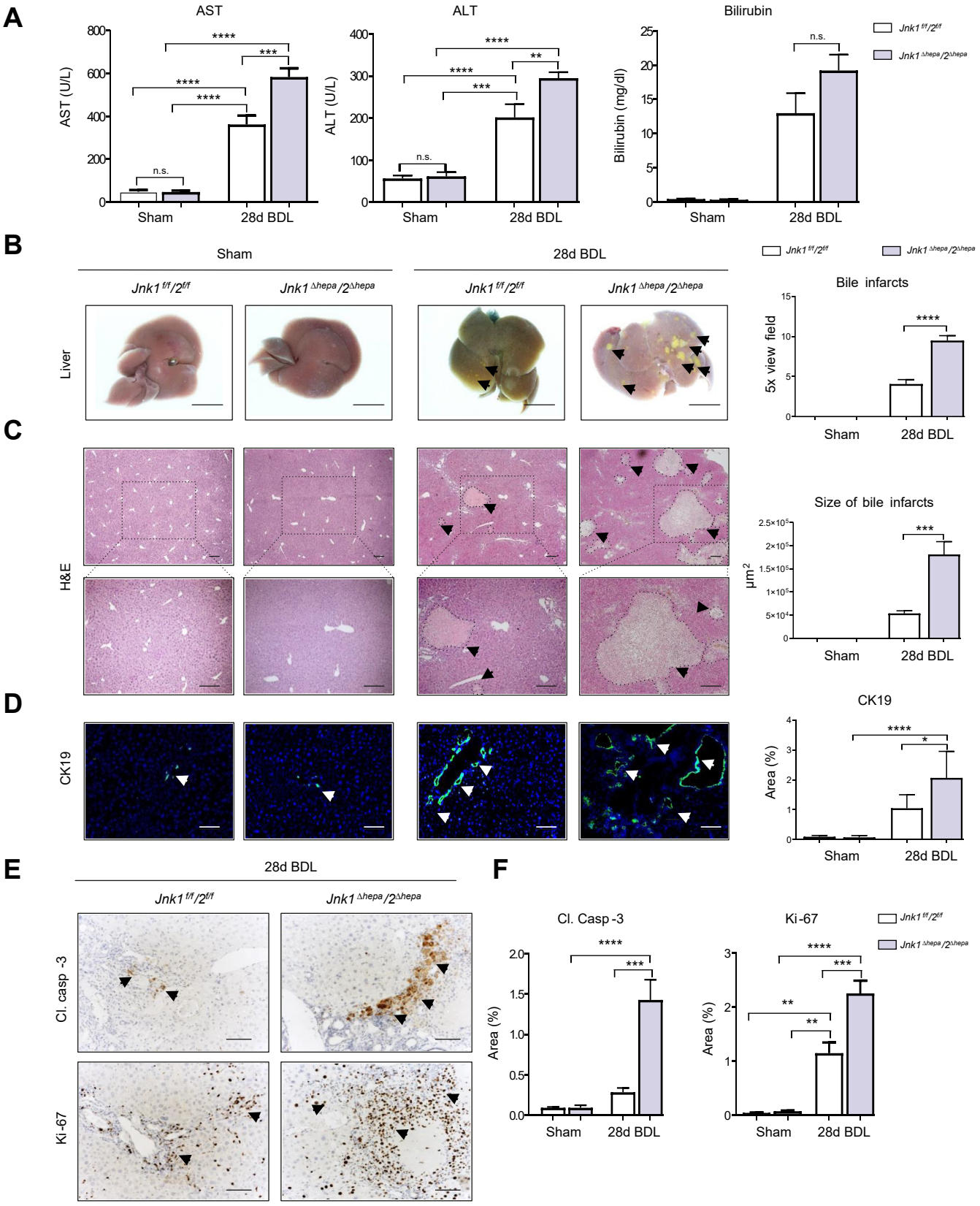

Fig. 3. Combined *Jnk1/2* loss in hepatocytes exacerbates BDL-induced liver damage, 28 days after BDL. (A) Serum AST and ALT levels were determined in $Jnk1^{f/f}/2^{f/f}$ (n = 5) and $Jnk1^{\Delta hepa}/2^{\Delta hepa}$ mice (n = 6), 28 days after BDL. Sham-operated mice were used as controls (n = 3). (B) Macroscopic appearance of $Jnk1^{f/f}/2^{f/f}$ and $Jnk1^{\Delta hepa}/2^{\Delta hepa}$ livers, 28 days after BDL surgery. Sham-operated mice were used as controls (n = 4). Scale bar = 1 cm. Arrows indicate yellow dots (bile infarcts) on the liver surface. (C) Representative H&E staining of paraffin liver sections from these mice are shown at different magnifications (5× in the upper

in biliary cells and NPCs of PSC and PBC livers compared with hepatocytes, as shown in Fig. 7A. By contrast, Apelin expression was nonexistent or barely visible in healthy control livers (Fig. 7A).

Inhibiting of Apelin signalling mitigates BDL-induced liver injury and fibrosis in Jnk-deficient mice

Our results strongly indicate that the Apelin–ApelinR pathway is involved in aggravating BDL-induced liver injury and fibrosis. Therefore, we aimed to inhibit Apelin signalling using an ApelinR antagonist (ML221). *Jnk1*$^{f/f}$/*2*$^{f/f}$ and *Jnk1*$^{\Delta hepa}$/*2*$^{\Delta hepa}$ mice were i.v. injected thrice weekly with ML221, and BDL was performed for 7 days (Fig. S7A). The ML221 inhibitor did not cause any relevant histopathological, serum biochemistry, or body weight alterations in sham-operated *Jnk1*$^{f/f}$/*2*$^{f/f}$ and *Jnk1*$^{\Delta hepa}$/*2*$^{\Delta hepa}$ mice (Fig. 7B–E and Fig. S7B–D). However, ML221 treatment reduced fibrosis (Fig. 7B–D) and mitigated cholestatic liver damage caused by BDL in *Jnk1*$^{f/f}$/*2*$^{f/f}$ mice (Fig. 7B–E). More importantly, this effect was more prominent in *Jnk1*$^{\Delta hepa}$/*2*$^{\Delta hepa}$ mice, resulting in a significant reduction of ductular fibrosis (Fig. 7B and C). ML221 also improved liver architecture (Fig. 7D) and significantly restored serum AST, ALT, and AP levels in *Jnk1*$^{\Delta hepa}$/*2*$^{\Delta hepa}$ BDL-treated mice to WT levels (Fig. 7E and Fig. S7C and D). These results strongly indicate the importance of the JNK–Apelin axis in promoting BDL-induced cholestatic liver injury.

Jnk1/2 knockdown in WT mice recapitulates the *Jnk1*$^{\Delta hepa}$/*2*$^{\Delta hepa}$ phenotype after BDL treatment

Hepatocyte-specific inhibition of JNK expression has a strong effect on acute and chronic cholestasis. Thus, we sought to alter *Jnk1/2* expression selectively in hepatocytes to see whether coordinated targeting of two different targets *in vivo* is feasible. The effective simultaneous knockdown of *Jnk1/2* at both the mRNA and protein levels in hepatocytes was first investigated. A single i.v. injection of siRNA against *Jnk1* and *Jnk2* that was LNP-encapsulated (*siJnk1/2*; 2:1 ratio; 0.75 mg/kg body weight) was given to WT mice. The same dose of siRNA against GFP was administered to the corresponding control group (*siGFP*). Importantly, compared with mice given the same dose of *siGFP*, mice given a single i.v. injection of *siJnk1/2* showed a considerable downregulation of JNK1 and JNK2 mRNA and protein expression (Fig. S7E and F).

Next, we assessed whether a *Jnk1/2* knockdown in WT mice recapitulates the phenotype as found in *Jnk1*$^{\Delta hepa}$/*2*$^{\Delta hepa}$ mice after BDL treatment. WT mice were injected with LNP *siJnk1/2* or *siGFP* followed by BDL for 2 days (Fig. S7G). *siGFP* BDL-treated livers showed JNK activation in almost all hepatic cell types including hepatocytes and cholangiocytes (Fig. S7H). By contrast, pJNK-positive hepatocytes but not cholangiocytes were absent in *siJnk1/2* BDL-treated mice (Fig. S7I) as presented by pJNK and CK19 immunostaining in serial sections (Fig. S7H and I). These data indicate that our lipid-encapsulated siRNA to knock down JNK is efficient and hepatocyte-specific. Compared with that in untreated controls, BDL significantly increased the mRNA expression of *Jnk1* and tends to increase the expression of *Jnk2* in *siGFP* BDL livers (Fig. S7E). Interestingly, BDL in *siJnk1/2* mice showed elevated serum ALT, AST, AP, and GLDH levels compared with those in *siGFP* WT mice (Fig. 7F). Additional analysis of *siJnk1/2* BDL mice revealed that they had more biliary infarcts than *siGFP* BDL mice (Fig. 7G and H).

These findings demonstrate that it is possible to modify the course of cholestatic liver disease by combined modulating JNK1/2 expression selectively in hepatocytes.

Discussion

The physiological and pathological functions of JNK signalling vary, and in part, contradictory functions in promoting not only cell survival and proliferation but also cell death have been reported.[3] In addition, JNKs regulate important biological functions, including liver regeneration, although this pathway can also be detrimental, for example, during carcinogenesis. Preclinical studies in animal models or human cells indicated that JNK inhibitors might be used to treat patients with different liver diseases.[17–20] However, the first human studies, for example, a phase II study to treat non-alcoholic steatohepatitis with the oral pan-JNK inhibitor CC-90001, failed and were stopped at an early stage. It is very likely that the balance of the cell-specific role was not specifically addressed, and major undesirable side effects occurred.

Another example is SP600125, the most commonly used ATP-competitive pan-JNK inhibitor *in vitro* and *in vivo*. SP600125 displayed cytotoxic and off-target effects and has been shown to lack specificity owing to its ability to randomly inhibit phosphorylation of all JNK substrates.[21] These data suggest that general JNK inhibition might generate major side effects and more likely a cell-type-specific JNK approach might be effective.

Recently, a specific effort has been made, not only to better understand the cell-specific role of JNKs but also to differentiate between combined and/or unique functions of *Jnk1* and *Jnk2* genes. We and others showed that JNK activation is not only limited to hepatocytes but also found in pro-fibrotic and inflammatory cells during liver disease progression in humans and mice.[5,7,22]

In the current study, we demonstrated that strong JNK activation is a conserved mechanism across species in cholestatic liver disease. We found in patients with cholestasis (namely, patients with PBC and PSC), as well as in murine models of cholestasis (*Mdr2*$^{-/-}$ mice and WT mice after BDL), JNK activation in not only hepatocytes and BECs but also in NPCs. These results strongly suggested that JNKs play a pivotal role in different cell compartments during cholestatic liver injury. However, functional studies addressing distinct cell types during liver disease are needed before targeted approaches modulating JNK activity on a therapeutic level can be recommended.

panel and 10× in the lower panel; scale bar = 200 μm). Arrows indicate necrotic areas. Number and size of bile infarcts in the same mice were quantified. (D) Frozen sections from *Jnk1*$^{f/f}$/*2*$^{f/f}$ and *Jnk1*$^{\Delta hepa}$/*2*$^{\Delta hepa}$ livers (n = 5) were stained for CK19 followed by immunofluorescence microscopy. Scale bar = 100 μm. Arrows indicate positive cells. Relative CK19-positive stained areas were quantified using ImageJ® software (National Institutes of Health, Bethesda, MD, USA). (E) Representative immunohistochemistry staining for Cl. Casp-3 (upper panel) and Ki-67 (lower panel) of paraffin sections from *Jnk1*$^{f/f}$/*2*$^{f/f}$ and *Jnk1*$^{\Delta hepa}$/*2*$^{\Delta hepa}$ livers (n = 5–6), 28 days after BDL. Scale bar = 100 μm. Arrows indicate positive cells. (F) Percentage of positive area per view field for Cl. Casp-3 and Ki-67 were quantified in the same livers using ImageJ® software (National Institutes of Health, Bethesda, MD, USA). Statistical evaluation was carried out by multicomparison one-way ANOVA followed by *post hoc* Bonferroni's test among three or more groups. Values are represented as mean ± SEM (*n*, not significant; **p* <0.05; ***p* <0.01; ****p* <0.001; *****p* <0.0001). ALT, alanine aminotransferase; AST, aspartate aminotransferase; BDL, bile duct ligation; CK19, cytokeratin 19; Cl. Casp-3, cleaved caspase 3; JNK, c-Jun-N-terminal kinase.

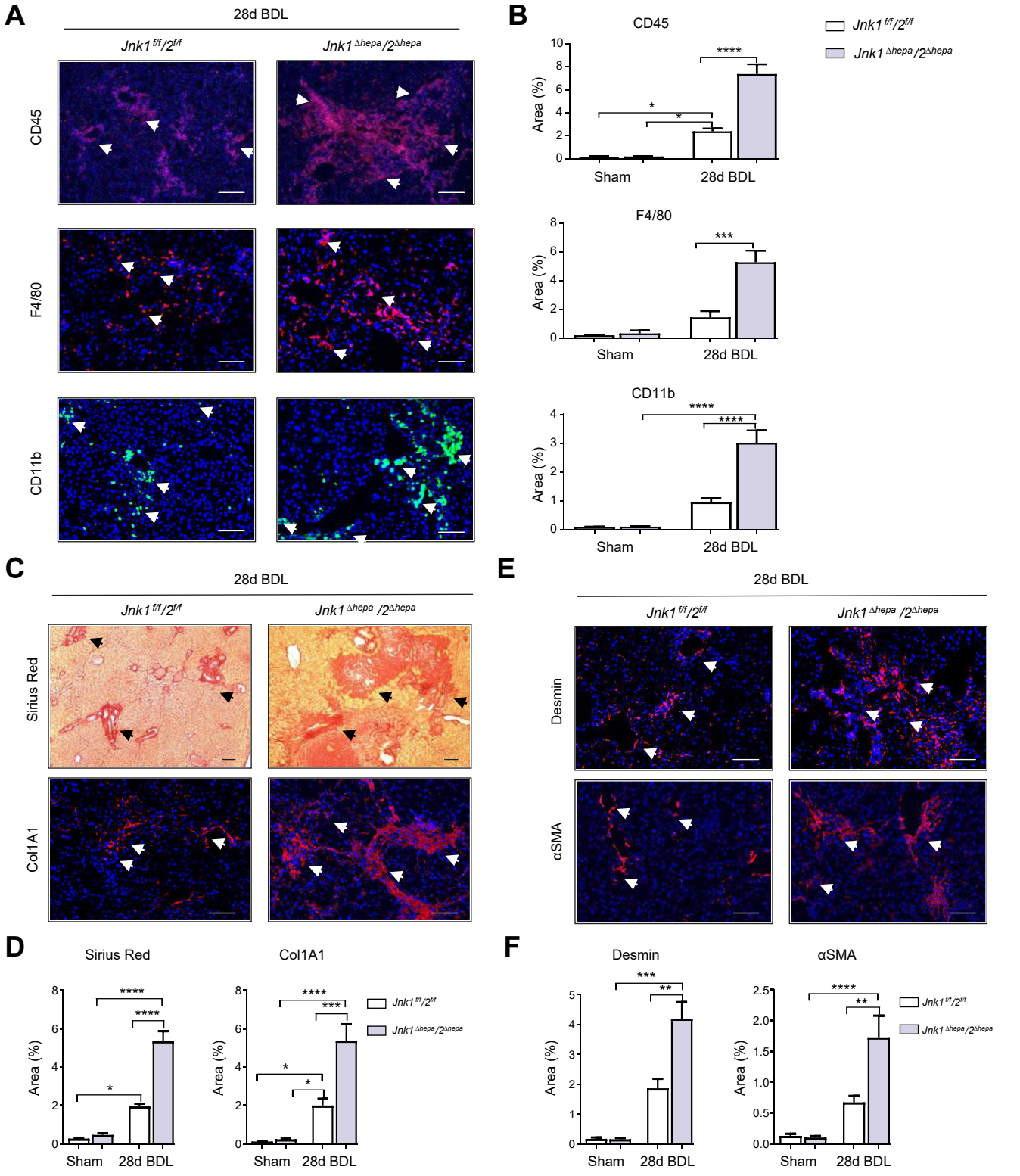

Fig. 4. Hepatic inflammatory response and fibrogenesis are aggravated in *Jnk1*$^{\Delta hepa}$/2$^{\Delta hepa}$ livers after BDL. (A) Representative immunofluorescence staining for CD45, F4/80, or CD11b on liver cryosections was performed in *Jnk1*$^{f/f}$/2$^{f/f}$ and *Jnk1*$^{\Delta hepa}$/2$^{\Delta hepa}$ livers (n = 5), 28 days after BDL. Scale bar = 100 μm. Arrows indicate positive cells. (B) Percentage of positive area per view field for CD45, F4/80, or CD11b were quantified in the same livers using ImageJ® software (National Institutes of Health, Bethesda, MD, USA). (C) Representative Sirius Red staining of paraffin sections and immunofluorescence staining of frozen sections with an antibody against Col1A1 were performed in *Jnk1*$^{f/f}$/2$^{f/f}$ and *Jnk1*$^{\Delta hepa}$/2$^{\Delta hepa}$ livers (n = 5), 28 days after BDL. Scale bar = 100 μm. Arrows indicate positive cells. (D) Quantifications of the Sirius Red- and Col1A1-positive area percentage using ImageJ® software (National Institutes of Health, Bethesda, MD, USA) are shown. (E) Immunofluorescence staining of frozen sections with antibodies against desmin and αSMA were performed in the same liver samples (n = 5). Scale bar = 100 μm. (F) Quantifications of desmin- and αSMA-positive area percentages using Image J® software are shown. Statistical evaluation was carried out by multicomparison one-way ANOVA followed by *post hoc* Bonferroni's test among three or more groups. Values are represented as mean ± SEM (*n*, not significant; **p* <0.05; ***p* <0.01; ****p* <0.001; *****p* <0.001). αSMA, alpha-smooth muscle actin; BDL, bile duct ligation; Col1A1, collagen 1A1; JNK, c-Jun-N-terminal kinase.

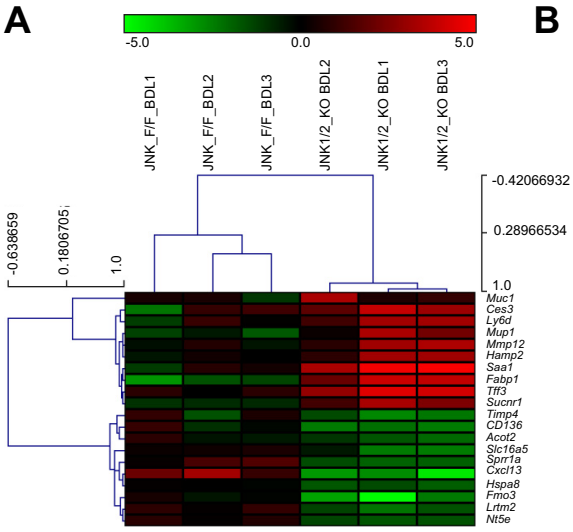

B

Jnk1$^{f/f}$/2$^{f/f}$ vs. *Jnk1* $^{\Delta hepa}$/2$^{\Delta hepa}$: BDL

Top canonical pathways	Top upstream regulators	Top molecules	
		Upregulated	Downregulated
Leukocyte signaling IL-17A Apelin liver signaling	LPS TNF β-estradiol IL-6	*Tff3* (+14.5) *Fabp1* (+10.1) *Mup1* (+9.0) *Ces3* (+7.8) *Sucnr1* (+5.3)	*Cxcl13* (-11.0) *Fmo3* (-5.7) *Cd163* (-3.2) *Nt5e* (-2.9)

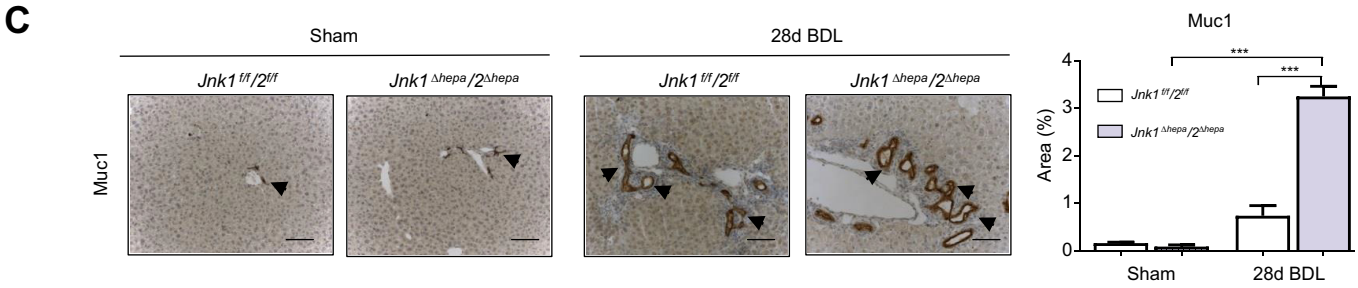

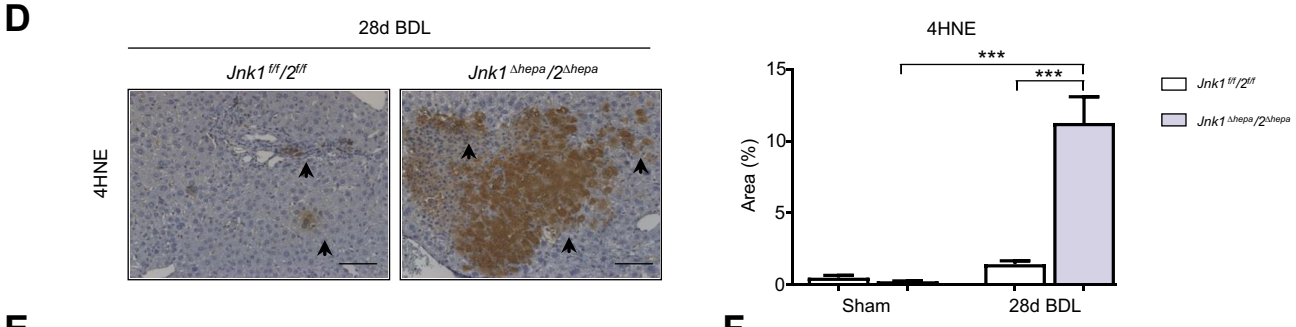

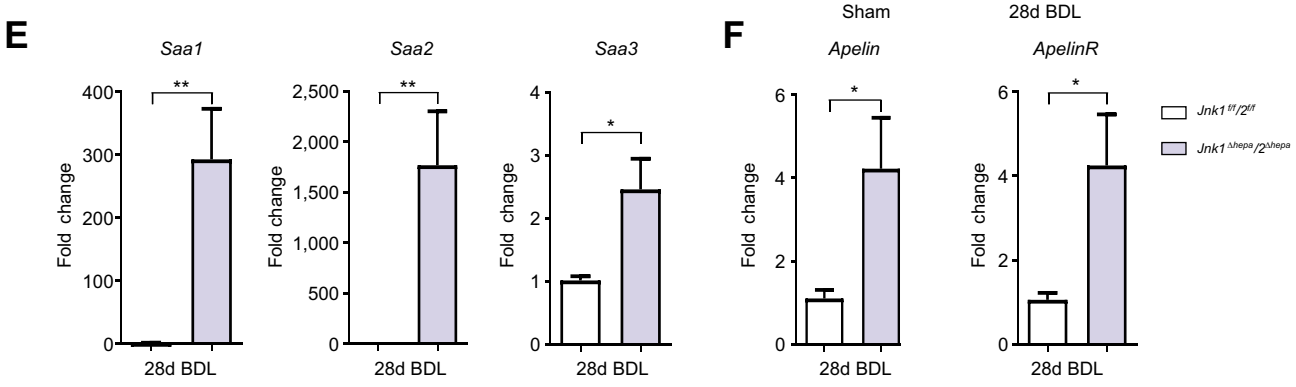

Fig. 5. *Jnk1/2*-dependent pathways during BDL-induced cholestatic liver injury. (A) Gene array analysis was performed in *Jnk1*$^{f/f}$/2$^{f/f}$ and *Jnk1*$^{\Delta hepa}$/2$^{\Delta hepa}$ livers, 28 days after BDL. Log_2 expression values of the individual mice were divided by the mean of the sham-operated mice. Log ratios were saved in a .txt file and analysed using the Multiple Experiment Viewer. Heat map of the top-regulated, upregulated, and downregulated genes (red, upregulated; green, downregulated, n = 3, -5.0 <fold change >5.0). (B) Ingenuity Pathway Analysis was performed in the same liver samples. The top canonical pathways (left panel), the top upstream regulators (middle panel), and the top up- and down-regulated genes (right panel) are represented. (C, D) Representative immunohistochemistry staining for Muc1 and 4HNE of paraffin sections from *Jnk1*$^{f/f}$/2$^{f/f}$ and *Jnk1*$^{\Delta hepa}$/2$^{\Delta hepa}$ livers (n = 5), 28 days after BDL. Scale bar = 100 μm. The positive area percentage was quantified using Image J® software. Arrows indicate positive cells. (E, F) mRNA expression analysis of acute-phase response genes (*Saa1, Saa2*, and *Saa3*), *Apelin*, and *ApelinR* was quantified by quantitative reverse-transcription PCR. Statistical evaluation was carried out by multicomparison one-way ANOVA followed by *post hoc* Bonferroni's test among three or more groups. Comparisons of two groups were analysed using an unpaired, two-tailed Student *t* test. Values are represented as mean ± SEM from five to six mice per group (*n*, not significant; **p* <0.05; ***p* <0.01; ****p* <0.001). 4HNE, 4-hydroxynonenal; ApelinR, Apelin receptor; BDL, bile duct ligation; JNK, c-Jun-N-terminal kinase; LPS, lipopolysaccharide; Muc1, mucin 1; TNF, tumour necrosis factor.

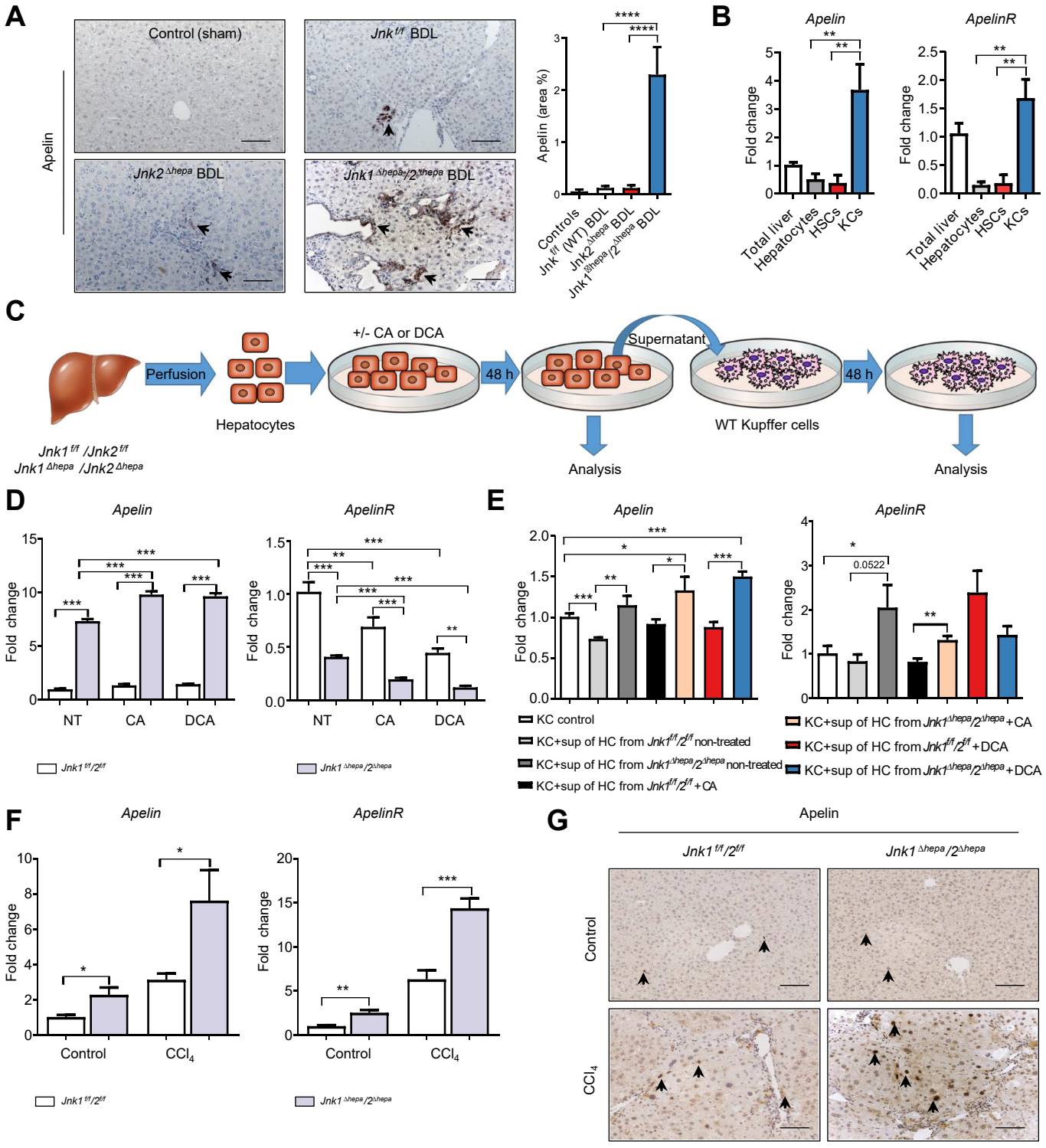

Fig. 6. JNK in hepatocytes regulates Apelin expression. (A) Representative immunohistochemistry staining for Apelin of paraffin sections from *Jnk$^{f/f}$* (WT), *Jnk2$^{\Delta hepa}$*, and *Jnk1$^{\Delta hepa}$/2$^{\Delta hepa}$* livers (n = 5), 28 days after BDL. Scale bar = 100 μm. Arrows indicate positive cells. Sham-operated mice were used as controls. The percentage of positive area per view field for Apelin were quantified in the same livers using ImageJ® software (National Institutes of Health, Bethesda, MD, USA). (B) mRNA expression analysis of *Apelin and ApelinR* in total liver, hepatocytes, HSCs, and KCs isolated from WT mice (n = 3) was quantified by quantitative reverse-transcription PCR. (C) Schematic view of the experimental design. (D) mRNA expression analysis of *Apelin and ApelinR* in *Jnk1$^{f/f}$/2$^{f/f}$* and *Jnk1$^{\Delta hepa}$/2$^{\Delta hepa}$* primary hepatocytes stimulated with or without CA and DCA (n = 6). (E) mRNA expression analysis of *Apelin and ApelinR* in isolated KCs from WT mice and stimulated with the culture supernatant of primary hepatocytes isolated from *Jnk1$^{f/f}$/2$^{f/f}$* and *Jnk1$^{\Delta hepa}$/2$^{\Delta hepa}$* livers and previously stimulated with or without CA and DCA (n = 6). (F) mRNA expression analysis of *Apelin and ApelinR* in *Jnk1$^{f/f}$/2$^{f/f}$* and *Jnk1$^{\Delta hepa}$/2$^{\Delta hepa}$* livers from CCl_4-treated mice (n = 5). (G) Representative immunohistochemistry staining for Apelin of paraffin sections from the same mice (n = 5). Scale bar = 100 μm. Arrows indicate positive cells. Oil-treated mice were used as controls. Statistical evaluation was carried out by multicomparison one-way ANOVA followed by *post hoc* Bonferroni's test among three or more groups. Values are represented as mean ± SEM (*p <0.05; **p <0.01; ***p <0.001). ApelinR, Apelin receptor; BDL, bile duct ligation; CA, cholic acid; CCl_4, carbon tetrachloride; DCA, deoxycholic acid; HC, hepatocyte; HSC, hepatic stellate cell; JNK, c-Jun-N-terminal kinase; NT, non-treated; KC, Kupffer cell; WT, wild-type.

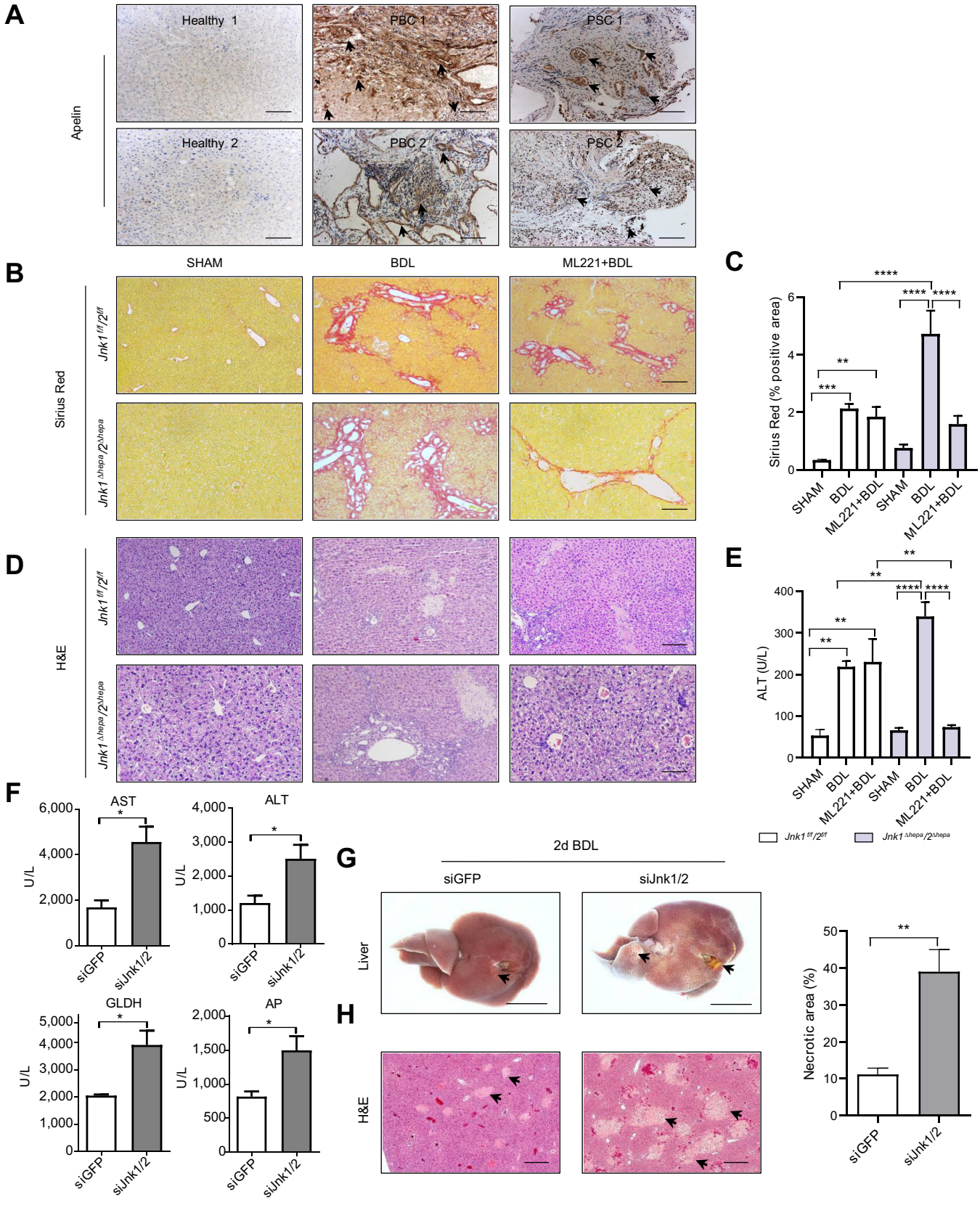

Fig. 7. Inhibiting Apelin signalling ameliorates cholestasis and *siRNA* against *Jnk1/2* recapitulates *Jnk1*$^{\Delta hepa}$/*2*$^{\Delta hepa}$ phenotype after BDL. (A) Representative immunohistochemistry staining for Apelin of human PBC and PSC liver sections (n = 3). Scale bar = 100 μm. Arrows indicate Apelin-positive cells. (B, C) *Jnk1*$^{f/f}$/*2*$^{f/f}$ and *Jnk1*$^{\Delta hepa}$/*2*$^{\Delta hepa}$ mice were treated with ML221 with/without BDL for 7 days (n = 4). SR staining from ML221 + BDL or sham-operated mice and positive area of fibrosis was calculated. Scale bars = 100 μm. (D) Representative H&E staining performed on paraffin liver sections. Scale bars = 100 μm. (E) Serum ALT levels of

Here, we aimed to define the role of JNKs in hepatocytes. In our earlier study, we showed that *Jnk1* deletion in hepatocytes has no impact on liver disease progression in the BDL model.[7] Therefore, we generated $Jnk2^{\Delta hepa}$ and combined $Jnk1^{\Delta hepa}/2^{\Delta hepa}$ animals. Interestingly, only $Jnk1^{\Delta hepa}/2^{\Delta hepa}$ animals, but not $Jnk2^{\Delta hepa}$ animals, developed a clearly pronounced phenotype, after acute and chronic BDL. These results demonstrate that *Jnk1* and *Jnk2* have redundant protective functions in hepatocytes during chronic cholestasis and can compensate for each other. However, if both genes are deleted specifically in hepatocytes, this results in an increased oxidative stress response triggering severe liver injury. Interestingly, we identified genes involved in energy metabolism (fat and glucose), which showed the strongest regulation. Hence, increased damage in $Jnk1^{\Delta hepa}/2^{\Delta hepa}$ hepatocytes after BDL may trigger a strong metabolic response very likely to cope with exacerbated liver injury.

BA accumulation as a result of cholestasis triggers an enhanced ductular reaction associated with increased levels of growth factors, reactive oxygen species, and cytokines contributing to the pathological condition.[16] IL-6 signalling is implicated in regulating the physiological and pathological function of BECs. Moreover, IL-6 promotes BEC protection by controlling mucin-associated proteins and trefoil factors (TFFs).[23,24] Consistently, our microarray analysis pointed towards increased oxidative stress burst and overexpression of the IL-6 pathway in response to hepatocytic JNK1/2 deletion, as we previously reported.[10] More importantly, our data demonstrated the protection of the mucosal epithelium as mucin and trefoil family members were strongly upregulated in the absence of hepatocytic JNK1/2. TFF peptides in the gastrointestinal tract increase the viscosity of mucins and help to protect epithelial linings from insults. Concomitantly, TFF1/3 are constitutively expressed and increased in pathologic biliary ducts.[25] Thus, strong TFF1/3 and Muc1 expression likely is a mechanism of repair in biliary neoductogenesis, which is exacerbated after loss of JNK1/2 in hepatocytes.

The Apelin/ApelinR system is expressed in various tissues including liver and has been shown to promote liver fibrosis, cholestasis, and cholangiocarcinoma.[16,26,27] Recently, Chen *et al.*[16] showed increased serum Apelin level in patients with PSC and demonstrated that the Apelin–ApelinR axis promotes increased oxidative stress and extracellular signal-regulated kinase signalling pathways triggering biliary epithelial proliferation and liver fibrosis. In line with these findings, we found increased Apelin expression in human PSC and PBC livers. In addition, our results showed increased 4-hydroxynonenal levels, a marker of lipid peroxidation and oxidative stress, as well as expression of Apelin and its receptor after BDL and CCl_4 treatment.

Interestingly, the cellular source of Apelin expression seems to be different in the two models. Although Apelin staining in CCl_4-treated $Jnk1^{\Delta hepa}/2^{\Delta hepa}$ livers was identified in hepatocytes and fibrous septa and was more intense in the fibrotic tissue most likely in HSCs as previously reported,[28,29] increased Apelin expression after BDL was prominent in cholangiocytes and NPCs of $Jnk1^{\Delta hepa}/2^{\Delta hepa}$ livers. This finding is supported by the observation that the Apelin–ApelinR axis is activated in different liver cell types during the progression of liver diseases,[30] suggesting that hepatocytic JNK regulates Apelin expression. Our *in vitro* results confirmed our hypothesis; thus, hepatocytes lacking JNK signalling exhibited increased *Apelin* expression in non-treated cells, which was further enhanced upon BA stimulation.

Yoshiya *et al.*[31] showed that Apelin signalling is expressed in KCs and inhibits liver regeneration in mice. Supporting this finding, our analysis of NPCs demonstrates increased expression of *Apelin* and *ApelinR* on KCs. We propose that Apelin signalling in KCs promotes hepatic cholestasis by inducing cholangiocytes. Interestingly, our results using supernatant transfer from hepatocytes to KC suggest a role of JNK signalling in hepatocytes in promoting *Apelin* expression in KCs via a paracrine manner, most likely by regulating Apelin expression in hepatocytes and/or by enhancing secretary factors release from JNK-deficient hepatocytes that induce Apelin expression in KCs.

Along with enhanced *Apelin* expression in KCs, increased hepatic macrophage infiltration was prominent in the periductal area of JNK-deficient mice. This is in agreement with a recent study from Guillot *et al.*[32] reporting that BA-activated macrophages promoted BEC proliferation and macrophage depletion reduced cholestasis and fibrogenesis after acute BEC injury. Collectively, Apelin-mediated crosstalk between KCs and BECs seems to be mediated by increased oxidative stress, and Apelin expression is triggered by JNK loss in hepatocytes during cholestasis.

Functionally, we demonstrated that inhibition of Apelin signalling by ML221 treatment ameliorated BDL-induced liver injury and fibrosis in $Jnk1^{f/f}/2^{f/f}$ mice, whereas this effect was more prominent in $Jnk1^{\Delta hepa}/2^{\Delta hepa}$ mice, indicating the importance of the JNK–Apelin axis during cholestasis progression.

By defining the mode of cell death, we observed that JNK deficiency in hepatocytes triggers increased cell death. Specifically, we found that apoptotic cell death was increased in $Jnk1^{\Delta hepa}/2^{\Delta hepa}$ livers and hepatocytes after BDL or BA treatment, respectively. These data suggested that during cholestatic liver injury, JNK1 and JNK2 activate anti-apoptotic signals most likely related to caspase-8-dependent cell death, as we recently showed that hepatocyte-specific caspase 8 deletion reduced JNK-derived apoptotic cell death after BDL[33] and further support the role of the Apelin–JNK axis in promoting Fas-induced liver injury.[34] In addition, $Jnk1^{\Delta hepa}/2^{\Delta hepa}$ mice displayed elevated compensatory proliferation, hepatic fibrogenesis, and inflammation after cholestatic-induced surgery. Altogether, these results suggest that targeting and modulating JNK1 and JNK2 function, specifically in hepatocytes, during cholestasis could be a promising therapeutic approach as already shown for JNK2.[35]

Finally, we aimed to interventionally modulate combined JNK expression in hepatocytes. Earlier, pharmacological JNK inhibitors improved disease progression in experimental models.[17,19] However, this approach lacks specificity on a cell-type and kinase-specific level.[18,21] Therefore, we established a combined *Jnk1/2* knockdown via siRNA. *Jnk1/2* siRNA-mediated nanodelivery in WT

sham-operated mice, BDL-treated, and ML221 + BDL-treated mice were calculated. (F) Serum AST, ALT, GLDH, and AP levels were determined in *siGFP* (n = 6) and *siJnk1/2* mice (n = 6), 2 days after BDL. (G) Macroscopic and (H) microscopic appearance of livers from the same mice. Arrows indicate yellow dots (bile infarcts) on the liver surface. Necrotic areas were quantified. Statistical evaluation was carried out by multicomparison one-way ANOVA followed by *post hoc* Bonferroni's test among three or more groups. Comparisons of two groups were analysed using an unpaired, two-tailed Student *t* test. Values are represented as mean ± SEM (**p* <0.05; ***p* <0.01; ****p* <0.001; *****p* <0.001). ALT, alanine aminotransferase; AP, alkaline phosphatase; AST, aspartate aminotransferase; BDL, bile duct ligation; JNK, c-Jun-N-terminal kinase; ML221, ApelinR antagonist; PBC, primary biliary cholangitis; PSC, primary sclerosing cholangitis; SR, Sirius Red.

BDL-treated mice increased liver injury as found in *Jnk1*$^{\Delta hepa}$/*2*$^{\Delta hepa}$ mice after BDL. Hence, both approaches, in contrast to the results by pharmacological inhibition, demonstrate that JNK1/2 have a pivotal protective role in hepatocytes during BDL-induced cholestatic liver injury. As we also found increased *Jnk1/2* expression after BDL in WT livers, we hypothesised that enhancing JNK1/2 expression in hepatocytes during cholestatic liver injury is likely an attractive therapeutic approach.

In summary, we defined the hepatocyte-specific protective role of JNK-dependent pathways during acute and chronic cholestatic liver injury via regulating the Apelin axis. Lack of combined JNK1/2 expression in hepatocytes triggers increased oxidative stress and pathways involved in energy metabolism and biliary repair. As dual targeting of JNK1/2 selectively in hepatocytes is feasible, future strategies to increase JNK1/2 expression in hepatocytes is likely beneficial.

Abbreviations

αSMA, alpha-smooth muscle actin; ALT, alanine aminotransferase; AP, alkaline phosphatase; ApelinR, Apelin receptor; AST, aspartate aminotransferase; BA, bile acid; BDL, bile duct ligation; BEC, biliary epithelial cell; CA, cholic acid; CCl_4, carbon tetrachloride; CK19, cytokeratin 19; Cl. Casp-3, cleaved caspase 3; COL1A1, collagen 1A1; DCA, deoxycholic acid; HSC, hepatic stellate cell; IL, interleukin; JNK, c-Jun-N-terminal kinase; *Jnk1*$^{\Delta hepa}$/*2*$^{\Delta hepa}$, mice carrying hepatocyte-specific deletion of *Jnk1* and *Jnk2*; *Jnk2*$^{\Delta hepa}$, mice carrying hepatocyte-specific deletion of Jnk2; KC, Kupffer cell; LNP, lipid nanoparticle; MAPK, mitogen-activated protein kinase; Mdr2, multidrug resistance 2; ML221, ApelinR antagonist; MMP, matrix metalloproteinase; Muc1, mucin 1; NPC, non-parenchymal cell; PBC, primary biliary cholangitis; PSC, primary sclerosing cholangitis; SAA, serum amyloid A; pJNK, phosphorylated JNK; siGFP, mice receiving siRNA to knock down GFP in hepatocytes; *siJnk1/2*, mice receiving siRNA to knock down *Jnk1* and *Jnk2* in hepatocytes; siRNA, small interfering RNA; SR, Sirius Red; TFF, trefoil factor; TNF, tumour necrosis factor; WT, wild-type.

Financial support

This work was supported by the German Research Foundation (DFG CRC 1382; Project-ID 403224013, Tr 285/10-2 and GRK 2375) to CT and by the Spanish Ministry of Science and Innovation (MICINN; PID2020-117941RB-I00), EXOHEP2-CM S2022/BMD-7409, and the HORIZON-HLTH-2022-STAYHLTH-02 under Agreement No. 101095679 to FJC. FJC is affiliated to the UCM groups 'Lymphocyte Immunobiology' No. 920631 (imas12-associated, Ref. IBL-6) and 'Liver Physiopathology' No. 070935. PB is supported by the German Research Foundation (DFG, Project IDs 322900939, 454024652, 432698239, and 445703531), European Research Council (ERC Consolidator Grant No. 101001791), and the Federal Ministry of Education and Research (STOP-FSGS-01GM2202). MB received support from the German Research Foundation (DFG) (BA6226/2-1), the Wilhelm Sander Foundation (2018.129.1), the COST Action Mye-InfoBank (CA20117), and the BMBF (16LW0143). CL was supported by a CSC stipend (202008320329). PS is supported by the German Research Foundation (DFG, Project IDs 418227595 and 403224013).

Conflicts of interest

The authors declare that they have no financial competing interests.

Please refer to the accompanying ICMJE disclosure forms for further details.

Authors' contributions

Performed BDL and analysed all the liver experiments, acquired the data, and drafted the manuscript: MRM. Helped with the BDL experiments: HS. Performed the apelin inhibitor experiments: HW. Generated siRNA-loaded lipid nanoparticles: MB, CL. Contributed human samples and clinical data and performed the histopathological analyses: JH, PB, BG, CR. Performed the gene array and analysed the data: MB. Contributed by performing human data analysis: PS. Provided the JNK mice: RJD. Reviewed the manuscript: FJC. Supervised the study, drafted the paper, provided funds, and critically reviewed the manuscript: CT.

Data availability statement

Data are available on reasonable request to the corresponding author.

Acknowledgements

The authors gratefully acknowledge Bettina Jansen, Stephanie Erschfeld, and Sonja Strauch for providing essential technical support with mice genotyping, providing histological sections of livers and performing H&E staining, Sirius Red staining, and immunostaining. In addition, the authors would like to thank the genomic facility of the Interdisciplinary Center for Clinical Research (IZKF) Aachen, RWTH-Aachen University, especially Bernd Denecke and Lin Gan for performing microarray experiments.

Supplementary data

Supplementary data to this article can be found online at https://doi.org/10.1016/j.jhepr.2023.100854.

References

Author names in bold designate shared co-first authorship

[1] Carbone M, Neuberger J. Liver transplantation in PBC and PSC: indications and disease recurrence. Clin Res Hepatol Gastroenterol 2011;35:446–454.
[2] Tag CG, Sauer-Lehnen S, Weiskirchen S, Borkham-Kamphorst E, Tolba RH, Tacke F, et al. Bile duct ligation in mice: induction of inflammatory liver injury and fibrosis by obstructive cholestasis. J Vis Exp 2015:52438.
[3] Seki E, Brenner DA, Karin M. A liver full of JNK: signaling in regulation of cell function and disease pathogenesis, and clinical approaches. Gastroenterology 2012;143:307–320.
[4] Wagner EF, Nebreda AR. Signal integration by JNK and p38 MAPK pathways in cancer development. Nat Rev Cancer 2009;9:537–549.
[5] Kluwe J, Pradere JP, Gwak GY, Mencin A, De Minicis S, Osterreicher CH, et al. Modulation of hepatic fibrosis by c-Jun-N-terminal kinase inhibition. Gastroenterology 2010;138:347–359.
[6] Yoshida K, Matsuzaki K, Mori S, Tahashi Y, Yamagata H, Furukawa F, et al. Transforming growth factor-beta and platelet-derived growth factor signal via c-Jun N-terminal kinase-dependent Smad2/3 phosphorylation in rat hepatic stellate cells after acute liver injury. Am J Pathol 2005;166:1029–1039.
[7] **Zhao G**, **Hatting M**, Nevzorova YA, Peng J, Hu W, Boekschoten MV, et al. Jnk1 in murine hepatic stellate cells is a crucial mediator of liver fibrogenesis. Gut 2014;63:1159–1172.
[8] Cubero FJ, Zoubek ME, Hu W, Peng J, Zhao G, Nevzorova YA, et al. Combined activities of *JNK1* and *JNK2* in hepatocytes protect against toxic liver injury. Gastroenterology 2016;150:968–981.
[9] Das M, Garlick DS, Greiner DL, Davis RJ. The role of JNK in the development of hepatocellular carcinoma. Genes Dev 2011;25:634–645.
[10] **Cubero FJ**, **Mohamed MR**, Woitok MM, Zhao G, Hatting M, Nevzorova YA, et al. Loss of c-Jun N-terminal kinase 1 and 2 function in liver epithelial cells triggers biliary hyperproliferation resembling cholangiocarcinoma. Hepatol Commun 2020;4:834–851.
[11] Manieri E, Folgueira C, Rodríguez ME, Leiva-Vega L, Esteban-Lafuente L, Chen C, et al. JNK-mediated disruption of bile acid homeostasis promotes intrahepatic cholangiocarcinoma. Proc Natl Acad Sci U S A 2020;117:16492–16499.
[12] Pollheimer MJ, Halilbasic E, Fickert P, Trauner M. Pathogenesis of primary sclerosing cholangitis. Best Pract Res Clin Gastroenterol 2011;25:727–739.
[13] Kouroumalis E, Samonakis D, Voumvouraki A. Biomarkers for primary biliary cholangitis: current perspectives. Hepat Med 2018;10:43–53.

[14] **Kuan CY**, **Yang DD**, Samanta Roy DR, Davis RJ, Rakic P, Flavell RA. The Jnk1 and Jnk2 protein kinases are required for regional specific apoptosis during early brain development. Neuron 1999;22:667–676.
[15] Kim KH, Chen CC, Alpini G, Lau LF. CCN1 induces hepatic ductular reaction through integrin αvβ5-mediated activation of NF-κB. J Clin Invest 2015;125:1886–1900.
[16] Chen LX, Zhou TH, White T, O'Brien A, Chakraborty S, Liangpunsakul S, et al. The Apelin–Apelin receptor axis triggers cholangiocyte proliferation and liver fibrosis during mouse models of cholestasis. Hepatology 2021;73:2411–2428.
[17] Cicuéndez B, Ruiz-Garrido I, Mora A, Sabio G. Stress kinases in the development of liver steatosis and hepatocellular carcinoma. Mol Metab 2021;50:101190.
[18] Tam SY, Law HK-W. JNK in tumor microenvironment: present findings and challenges in clinical translation. Cancers 2021;13:2196.
[19] Garg R, Kumariya S, Katekar R, Verma S, Goand UK, Gayen JR. JNK signaling pathway in metabolic disorders: an emerging therapeutic target. Eur J Pharmacol 2021;901:174079.
[20] Yung JHM, Giacca A. Role of c-Jun N-terminal Kinase (JNK) in obesity and type 2 diabetes. Cell 2020;9:706.
[21] **Wu QH**, **Wu WD**, Jacevic V, Franca TCC, Wang X, Kuca K. Selective inhibitors for JNK signalling: a potential targeted therapy in cancer. J Enzym Inhib Med Chem 2020;35:574–583.
[22] Toivola DM, Ku NO, Resurreccion EZ, Nelson DR, Wright TL, Omary MB. Keratin 8 and 18 hyperphosphorylation is a marker of progression of human liver disease. Hepatology 2004;40:459–466.
[23] Nozaki I, Lunz 3rd JG, Specht S, Park JI, Giraud AS, Murase N, et al. Regulation and function of trefoil factor family 3 expression in the biliary tree. Am J Pathol 2004;165:1907–1920.
[24] Jiang GX, Zhong XY, Cui YF, Liu W, Tai S, Wang ZD, et al. IL-6/STAT3/TFF3 signaling regulates human biliary epithelial cell migration and wound healing in vitro. Mol Biol Rep 2010;37:3813–3818.
[25] Sasaki M, Tsuneyama K, Saito T, Kataoka H, Mollenhauer J, Poustka A, et al. Site-characteristic expression and induction of trefoil factor family 1, 2 and 3 and malignant brain tumor-1 in normal and diseased intrahepatic bile ducts relates to biliary pathophysiology. Liver Int 2004;24:29–37.
[26] Huang S, Chen L, Lu L, Li L. The apelin–APJ axis: a novel potential therapeutic target for organ fibrosis. Clin Chim Acta 2016;456:81–88.
[27] Hall C, Ehrlich L, Venter J, O'Brien A, White T, Zhou TH, et al. Inhibition of the apelin/apelin receptor axis decreases cholangiocarcinoma growth. Cancer Lett 2017;386:179–188.
[28] Melgar-Lesmes P, Casals G, Pauta M, Ros J, Reichenbach V, Bataller R, et al. Apelin mediates the induction of profibrogenic genes in human hepatic stellate cells. Endocrinology 2010;151:5306–5314.
[29] Yokomori H, Oda M, Yoshimura K, Machida S, Kaneko F, Hibi T. Overexpression of apelin receptor (APJ/AGTRL1) on hepatic stellate cells and sinusoidal angiogenesis in human cirrhotic liver. J Gastroenterol 2011;46:222–231.
[30] Lv X, Kong J, Chen WD, Wang YD. The role of the apelin/APJ system in the regulation of liver disease. Front Pharmacol 2017;8:221.
[31] Yoshiya S, Shirabe K, Imai D, Toshima T, Yamashita Y, Ikegami T, et al. Blockade of the apelin-APJ system promotes mouse liver regeneration by activating Kupffer cells after partial hepatectomy. J Gastroenterol 2015;50:573–582.
[32] Guillot A, Guerri L, Feng D, Kim SJ, Ahmed YA, Paloczi J, et al. Bile acid-activated macrophages promote biliary epithelial cell proliferation through integrin αvβ6 upregulation following liver injury. J Clin Invest 2021;131:e132305.
[33] **Cubero FJ**, **Peng J**, Liao L, Su H, Zhao G, Eugenio Zoubek M, et al. Inactivation of caspase 8 in liver parenchymal cells confers protection against murine obstructive cholestasis. J Hepatol 2018;69:1326–1334.
[34] Yasuzaki H, Yoshida S, Hashimoto T, Shibata W, Inamori M, Toya Y, et al. Involvement of the apelin receptor APJ in Fas-induced liver injury. Liver Int 2013;33:118–126.
[35] Gunawan BK, Liu ZX, Han D, Hanawa N, Gaarde WA, Kaplowitz N. c-Jun N-terminal kinase plays a major role in murine acetaminophen hepatotoxicity. Gastroenterology 2006;131:165–178.
[36] Nakanuma Y, Zen Y, Harada K, Sasaki M, Nonomura A, Uehara T, et al. Application of a new histological staging and grading system for primary biliary cirrhosis to liver biopsy specimens: Interobserver agreement. Pathol Int 2010;60:167–174.
[37] Batts KP, Ludwig J. Chronic hepatitis. An update on terminology and reporting. Am J Surg Pathol 1995;19:1409–1417.